Atmos. Chem. Phys. Discuss., 6, 2965–3047, 2006
www.atmos-chem-phys-discuss.net/6/2965/2006/

Atmospheric Chemistry and Physics Discussions

Multi-model ensemble simulations of tropospheric NO_2 compared with GOME retrievals for the year 2000

T. P. C. van Noije[1], H. J. Eskes[1], F. J. Dentener[2], D. S. Stevenson[3], K. Ellingsen[4], M. G. Schultz[5], O. Wild[6,7], M. Amann[8], C. S. Atherton[9], D. J. Bergmann[9], I. Bey[10], K. F. Boersma[1], T. Butler[11], J. Cofala[8], J. Drevet[10], A. M. Fiore[12], M. Gauss[4], D. A. Hauglustaine[13], L. W. Horowitz[12], I. S. A. Isaksen[4], M. C. Krol[2,14], J.-F. Lamarque[15], M. G. Lawrence[11], R. V. Martin[16,17], V. Montanaro[18], J.-F. Müller[19], G. Pitari[18], M. J. Prather[20], J. A. Pyle[7], A. Richter[21], J. M. Rodriguez[22], N. H. Savage[7], S. E. Strahan[22], K. Sudo[6], S. Szopa[13], and M. van Roozendael[19]

[1]Royal Netherlands Meteorological Institute, De Bilt, The Netherlands
[2]Joint Research Centre, Institute for Environment and Sustainability, Ispra, Italy
[3]University of Edinburgh, School of Geosciences, Edinburgh, UK
[4]University of Oslo, Department of Geosciences, Oslo, Norway
[5]Max Planck Institute for Meteorology, Hamburg, Germany
[6]Frontier Research Center for Global Change, JAMSTEC, Yokohama, Japan
[7]University of Cambridge, Centre for Atmospheric Science, UK
[8]International Institute for Applied Systems Analysis, Laxenburg, Austria
[9]Lawrence Livermore National Laboratory, Atmospheric Science Division, Livermore, USA

[10] Ecole Polytechnique Fédéral de Lausanne, Switzerland
[11] Max Planck Institute for Chemistry, Mainz, Germany
[12] Geophysical Fluid Dynamics Laboratory, NOAA, Princeton, New Jersey, USA
[13] Laboratoire des Sciences du Climat et de l'Environnement, Gif-sur-Yvette, France
[14] Space Research Organisation Netherlands, Utrecht, The Netherlands
[15] National Center of Atmospheric Research, Atmospheric Chemistry Division, Boulder, Colorado, USA
[16] Department of Physics and Atmospheric Science, Dalhousie University, Halifax, Nova Scotia, Canada
[17] Smithsonian Astrophysical Observatory, Cambridge, Massachusetts, USA
[18] Università L'Aquila, Dipartimento di Fisica, L'Aquila, Italy
[19] Belgian Institute for Space Aeronomy, Brussels, Belgium
[20] Department of Earth System Science, University of California, Irvine, USA
[21] Institute of Environmental Physics, University of Bremen, Bremen, Germany
[22] Goddard Earth Sciences and Technology Center, Maryland, Washington, DC, USA

Received: 16 December 2005 – Accepted: 23 January 2006 – Published: 12 April 2006

Correspondence to: T. P. C. van Noije (noije@knmi.nl)

Abstract

We present a systematic comparison of tropospheric NO_2 from 17 global atmospheric chemistry models with three state-of-the-art retrievals from the Global Ozone Monitoring Experiment (GOME) for the year 2000. The models used constant anthropogenic emissions from IIASA/EDGAR3.2 and monthly emissions from biomass burning based on the 1997–2002 average carbon emissions from the Global Fire Emissions Database (GFED). Model output is analyzed at 10:30 local time, close to the overpass time of the ERS-2 satellite, and collocated with the measurements to account for sampling biases due to incomplete spatiotemporal coverage of the instrument. We assessed the importance of different contributions to the sampling bias: correlations on seasonal time scale give rise to a positive bias of 30–50% in the retrieved annual means over regions dominated by emissions from biomass burning. Over the industrial regions of the eastern United States, Europe and eastern China the retrieved annual means have a negative bias with significant contributions (between –25% and +10% of the NO_2 column) resulting from correlations on time scales from a day to a month. We present global maps of modeled and retrieved annual mean NO_2 column densities, together with the corresponding ensemble means and standard deviations for models and retrievals. The spatial correlation between the individual models and retrievals are high, typically in the range 0.81–0.93 after smoothing the data to a common resolution. On average the models underestimate the retrievals in industrial regions, especially over eastern China and over the Highveld region of South Africa, and overestimate the retrievals in regions dominated by biomass burning during the dry season. The discrepancy over South America south of the Amazon disappears when we use the GFED emissions specific to the year 2000. The seasonal cycle is analyzed in detail for eight different continental regions. Over regions dominated by biomass burning, the timing of the seasonal cycle is generally well reproduced by the models. However, over Central Africa south of the Equator the models peak one to two months earlier than the retrievals. We further evaluate a recent proposal to reduce the NO_x emission

factors for savanna fires by 40% and find that this leads to an improvement of the amplitude of the seasonal cycle over the biomass burning regions of Northern and Central Africa. In these regions the models tend to underestimate the retrievals during the wet season, suggesting that the soil emissions are higher than assumed in the models. In general, the discrepancies between models and retrievals cannot be explained by a priori profile assumptions made in the retrievals, neither by diurnal variations in anthropogenic emissions, which lead to a marginal reduction of the NO_2 abundance at 10:30 local time (by 2.5–4.1% over Europe). Overall, there are significant differences among the various models and, in particular, among the three retrievals. The discrepancies among the retrievals (10–50% in the annual mean over polluted regions) indicate that the previously estimated retrieval uncertainties have a large systematic component. Our findings imply that top-down estimations of NO_x emissions from satellite retrievals of tropospheric NO_2 are strongly dependent on the choice of model and retrieval.

1 Introduction

Nitrogen dioxide (NO_2) plays a key role in tropospheric chemistry with important implications for air quality and climate change. On the one hand, tropospheric NO_2 is essential for maintaining the oxidizing capacity of the atmosphere. Photolysis of NO_2 during daytime is the major source of ozone (O_3) in the troposphere and photolysis of O_3 in turn initializes the production of the hydroxyl radical (OH), the main cleansing agent of the atmosphere. On the other hand, NO_2 as well as O_3 are toxic to the biosphere and may cause respiratory problems for humans. Moreover, NO_2 may react with OH to form nitric acid (HNO_3), one of the main components of acid rain. As a greenhouse gas, NO_2 contributes significantly to radiative forcing over industrial regions, especially in urban areas (Solomon et al., 1999; Velders et al., 2001). Although the direct contribution of tropospheric NO_2 to global warming is relatively small, emissions of nitrogen oxides ($NO_x \equiv NO+NO_2$) affect the global climate indirectly by perturbing O_3 and methane (CH_4) concentrations. Overall, indirect long-term global radiative

cooling due to decreases in CH_4 and O_3 dominates short-term warming from regional O_3 increases (Wild et al., 2001; Derwent et al., 2001; Berntsen et al., 2005).

The main sources of tropospheric NO_x are emissions from fossil fuel combustion, mostly from power generation, road transport as well as marine shipping, and industry. Other important surface sources are emissions from biomass burning, mostly from savanna fires and tropical agriculture, and from microbial activity in soils; important sources in the free troposphere are emissions from lightning and aircraft. Minor sources are due to oxidation of ammonia (NH_3) by the biosphere and transport from the stratosphere. By far the majority of the NO_x is emitted as NO, but photochemical equilibration with NO_2 takes place within a few minutes. The principal sink of tropospheric NO_x is oxidation to HNO_3 by reaction of NO_2 with OH during daytime and by reaction of NO_2 with O_3 followed by hydrolysis of N_2O_5 on aerosols at night (Dentener and Crutzen, 1993; Evans and Jacob, 2005). The resulting NO_x lifetime in the planetary boundary layer varies from several hours in the tropics to 1–2 days in the extratropics during winter (Martin et al., 2003b) and increases to a few days in the upper troposphere. Long-range transport of NO_x may take place in the form of peroxyacetylnitrate (PAN), which is formed by photochemical oxidation of hydrocarbons in the presence of NO_x. As PAN is stable at low temperatures, it may be transported over large distances through the middle and upper troposphere and release NO_x far from its source by thermal decomposition during subsidence.

Because of the relatively heterogeneous distribution of its sources and sinks in combination with its short lifetime, the concentration of tropospheric NO_x is highly variable in space and time. Monitoring of NO_2 therefore requires covering a broad spectrum of spatial and temporal scales, using a combination of ground-based, air-borne as well as satellite measurements. During the last decade, observations from space have provided a wealth of information on the global and regional distribution of NO_2 on daily to multi-annual time scales. We now have nearly 10 years of tropospheric NO_2 data from the Global Ozone Monitoring Experiment (GOME) instrument on board the second European Remote Sensing (ERS-2) satellite, which was launched by the European Space

Agency (ESA) in April 1995. ERS-2 flies in a sun-synchronous polar orbit, crossing the equator at 10:30 local time. GOME is a nadir-viewing spectrometer operating in the ultraviolet and visible part of the spectrum, and has a forward-scan ground pixel size of 320 km across track by 40 km along track. Global coverage of the observations is reached within three days. Global tropospheric NO_2 columns have been retrieved from GOME for the period January 1996–June 2003; since 22 June 2003 data coverage is limited to Europe, the North Atlantic, western North America, and the Arctic (due to failure of the ERS-2 tape recorder). Higher resolution tropospheric NO_2 retrieval data have recently become available from the Scanning Imaging Absorption Spectrometer for Atmospheric Chartography (SCIAMACHY) instrument on board the ESA Envisat satellite (launched in March 2002) and from the Ozone Monitoring Instrument (OMI) on board the NASA Earth Observing System (EOS) Aura satellite (launched in July 2004).

GOME NO_2 data have proven very useful for monitoring tropospheric composition and air pollution on global to regional scales. Beirle et al. (2003), for instance, analyzed the weekly cycle in tropospheric NO_2 column densities from GOME for 1996–2001. Over different regions of the world as well as over individual cities, they found a clear signal of the "weekend effect", with reductions on rest days typically between 25–50%. Another outstanding example is the analysis of inter-annual variability in biomass burning and the detection of trends in industrial emissions on the basis of tropospheric NO_2 column densities from GOME over the period 1996–2002 (Richter et al., 2004, 2005). The large increase seen by GOME over eastern China has been shown to be consistent with time series from SCIAMACHY for the years 2002–2004 (Richter et al., 2005; van der A et al., 2006) and is supported by validation with ground-based measurements of total NO_2 column densities at three nearby sites in Central and East Asia in combination with independent satellite observations of stratospheric column densities (Irie et al., 2005).

Retrievals of tropospheric NO_2 column densities from GOME have also been compared with aircraft measurements of NO_2 profiles over Austria (Heland et al., 2002) and the southeastern United States (Martin et al., 2004), with ground-based observa-

tions of tropospheric column densities as well as in-situ measurements of NO_2 concentrations in the Po basin (Petritoli et al., 2004), and with in-situ measurements from approximately 100 ground stations in the Lombardy region (northern Italy) (Ordóñez et al., 2006). These studies all report reasonably good agreement under cloud free conditions. However, for quantitative interpretation of the results, it is important to realize that in most cases the satellite retrievals are not directly compared with in-situ aircraft or surface measurements. Hence, such validations typically involve assumptions on boundary layer mixing or the shape of the vertical profile. If the in-situ measurements are done with conventional molybdenum converters, an additional difficulty arises from the fact that these are sensitive to oxidized nitrogen compounds other than NO_2, such as HNO_3 and PAN, as well. The surface measurements by Ordóñez et al. (2006) have therefore been corrected using simultaneous measurements with a photolytic converter, which is highly specific for NO_2.

Given the uncertainties involved in the quantitative validation of the NO_2 retrievals from space, one may question the accuracy of the present state-of-the-art satellite products. Systematic analyses of the uncertainties involved in retrieving tropospheric NO_2 column densities have been presented in the literature (Boersma et al., 2004; Martin et al., 2002, 2003b; Konovalov, 2005). Bottom-up estimates of the errors involved in the consecutive steps of the retrieval indicate that the uncertainty in the vertical column density from GOME is typically 35–60% on a monthly basis over regions where the tropospheric contribution dominates the stratospheric part and can be much larger over remote regions (Boersma et al., 2004).

Despite these large uncertainties, tropospheric NO_2 retrievals from GOME and SCIAMACHY have been used in several studies for assessing the performance of atmospheric chemistry models and for identifying deficiencies in the NO_x emission inventories assumed in these models. Leue et al. (2001) developed image-processing techniques for analyzing global NO_2 maps from GOME and presented methods for separating the tropospheric and stratospheric contributions and for estimating the lifetime of NO_x in the troposphere, which allowed them to determine regional NO_x source

strengths. Velders et al. (2001) compared these image-processing techniques with another approach for separating the tropospheric and stratospheric contributions, known as the reference sector or tropospheric excess method, and evaluated various aspects of the retrievals using output from the global chemistry transport models IMAGES and MOZART. Two recent studies overestimated tropospheric NO_2 over polluted regions compared to GOME, but neglected hydrolysis of N_2O_5 on tropospheric aerosols (Lauer et al., 2002; Savage et al., 2004). To give an indication of the importance of N_2O_5 hydrolysis: Dentener and Crutzen (1993) showed that tropospheric NO_x concentrations at middle and high latitudes could be reduced by up to 80% in winter and 20% in summer, and in the tropics and subtropics by 10–30%. Kunhikrishnan et al. (2004a, b) characterized tropospheric NO_x over Asia, with a focus on India and the Indian Ocean, using the MATCH-MPIC global model and GOME NO_2 columns retrieved by the Institute of Environmental Physics (IUP) of the University of Bremen. Konovalov et al. (2005) made a comparison of summertime tropospheric NO_2 over Western and Eastern Europe from the regional air quality model CHIMERE with a more recent version of the GOME retrieval by the Bremen group and found reasonable agreement after correcting for the upper tropospheric contribution from NO_2 above 500 hPa, the model top of CHIMERE. A detailed analysis for Western Europe was presented by Blond et al. (2006)[1], who compared tropospheric NO_2 from a vertically extended version (up to 200 hPa) of CHIMERE with high-resolution column observations from SCIAMACHY as retrieved by BIRA/KNMI.

Other studies have taken a more ambitious approach and related the discrepancies between modeled and retrieved tropospheric NO_2 columns to errors in the bottom-up NO_x emission inventories assumed in the model. Martin et al. (2003b) presented an improved version of the retrieval by the Smithsonian Astrophysical Observatory (SAO)

[1]Blond, N., Boersma, K. F., Eskes, H. J., van der A, R., van Roozendael, M., de Smedt, I., Bergametti, G., and Vautard, R.: Intercomparison of SCIAMACHY nitrogen dioxide observations, in-situ measurements and air quality modelling results over Western Europe, J. Geophys. Res., in review, 2006.

and Harvard University (Martin et al., 2002) including a correction scheme to account for the presence of aerosols, and compared it with column output, sampled at the GOME overpass time, from the global chemistry transport model GEOS-CHEM. They argued that for top-down estimation of surface NO_x emissions over land from GOME tropospheric NO_2 columns, it is not necessary to account for horizontal transport of NO_x, because of the relatively short lifetime of NO_x in the continental boundary layer. In the inversion presented by these authors, top-down estimates are simply derived by a local scaling of the a priori assumed emissions by the ratio between the observed and the modeled column densities. The final a posteriori emission estimates follow by combining the resulting top-down estimates with the a priori assumed emissions, weighted by the relative errors in both. The corresponding a posteriori errors were found to be substantially smaller than the a priori errors throughout the world, with especially large error reductions over remote regions including Africa, the Middle East, South Asia and the western United States.

The same inverse modeling approach was further exploited by Jaeglé et al. (2004), who focused on NO_x emissions over Africa in the year 2000 and presented evidence of strongly enhanced emissions from soils over the Sahel during the rainy season. Recently the analysis was extended to other continental regions, for which a partitioning of NO_x sources between fuel combustion (fossil fuel and biofuel), biomass burning and soil emissions was derived (Jaeglé et al., 2005). A more sophisticated inversion method was developed by Müller and Stavrakou (2005), who combined tropospheric NO_2 column data from GOME with ground-based CO observations to simultaneously optimize the regional emission of NO_x and CO for the year 1997 using the adjoint of the IMAGES model. The GOME retrieval used in this study is similar to the one used by Konovalov (2005). As pointed out by Müller and Stavrakou (2005), their a posteriori emission estimates differ significantly from the estimates presented by Martin et al. (2003b), for instance over South America, Africa, and South Asia. According to the authors these discrepancies might be partly due to the different retrieval approaches, but are probably mostly related to differences between the GEOS-CHEM and the IM-

AGES model. It is therefore important to realize that the emission estimates derived from inverse modeling are sensitive to biases in individual models and retrievals.

The diversity of models and retrieval products renders it difficult to draw firm conclusions on whether and where models and retrievals agree or rather disagree beyond their respective uncertainties. A detailed and systematic comparison of models and satellite products was until now not available. Most studies mentioned above have evaluated the performance of an individual model using one of the satellite products from the different retrieval groups; Velders et al. (2001) compared two different models with two different retrievals. In this paper we will present a more systematic comparison using an ensemble of models and the three main GOME retrieval products that are currently available. We take advantage of the model intercomparison described by Dentener et al. (2006a) and Stevenson et al. (2006), in which a large number of models participated in 26 different configurations. A subset of 17 models out of these provided NO_2 fields for comparison with GOME observations for the year 2000. The model intercomparison offers the advantage that all models used prescribed state-of-the-art emission estimates, facilitating the analysis of systematic differences.

The outline of this paper is as follows. We begin with an overview of the most relevant aspects of the different retrieval methods (Sect. 2), followed by a description of the models setup (Sect. 3). Details of the method of comparison between models and retrievals are given in Sect. 4. Results of this comparison are presented in Sect. 5. Additional simulations that have been performed to assess the sensitivity of the results to assumptions on emissions from biomass burning and to estimate the impact of diurnal variations in anthropogenic emissions are described in Sect. 6. Finally, we conclude in Sect. 7 with a summary and discussion of our main findings.

2 GOME retrievals

The modelled NO_2 distributions are compared with three state-of-the art retrieval schemes which have been developed independently by the retrieval groups at Bremen

University (Richter and Burrows, 2002; Richter et al., 2005), Dalhousie University/SAO (Martin et al., 2003b) and BIRA/KNMI (Boersma et al., 2004). The three groups use the same general approach to the retrieval, based on a spectral fit of NO_2 to a reflectance spectrum giving an observed column, the subsequent estimation of the stratospheric contribution to the observed column and the use of a chemistry-transport model to provide tropospheric a priori NO_2 profile shapes as input for the retrieval. However, the details of the retrievals – the fitting, chemistry transport model, stratospheric background estimate, radiative transfer code, cloud retrieval, albedo maps and aerosol treatment – all differ (see Table A1). Consequently the intercomparison of the three retrievals becomes interesting, since the differences in the tropospheric column estimates can provide a posteriori information on intrinsic retrieval uncertainties.

In all three retrievals the observed differential features – that vary rapidly with wavelength – in the reflectance spectrum are matched with a set of reference cross sections of species absorbing in a chosen wavelength window and a reference spectrum accounting for Raman scattering. The amplitude of the spectral features is a measure of the tracer amount along the light path, called the slant column. The slant column is then converted into a vertical tracer column by dividing it by an air-mass factor (AMF) computed with a radiative transfer model. In fact, the NO_2 retrieval consists of three steps:

1. Spectral fit: The NO_2 spectral fits are performed with software developed independently at Bremen (Burrows et al., 1999; Richer and Burrows, 2002), SAO (Chance et al., 1998; Martin, et al., 2002) and BIRA/IASB (Vandaele et al., 2005). The European retrievals use the Differential Optical Absorption Spectroscopy (DOAS) technique; the SAO algorithm uses a direct spectral fit. The quoted precision is similar for the three retrievals. A comparison of the GOME Data Processor (GDP) version 2.7 columns with columns retrieved by the Heidelberg group (Leue et al., 2001) suggests a precision of about 4×10^{14} molecules cm^{-2} (Boersma et al., 2004). For typical columns of 2×10^{16} molecules cm^{-2} in polluted areas, this implies uncertainties of only a few percent. The fitting noise becomes especially

important and dominant for clean areas with tropospheric NO_2 columns less than 1×10^{15} molecules cm^{-2}, especially near the equator where the path length of the light is small.

2. Stratosphere: The total measurement is often dominated by a large background due to NO_2 in the stratosphere. Because nitrogen oxides are well mixed in the stratosphere they can be efficiently distinguished from the tropospheric contribution which is present near to the localized NO sources. The Dalhousie/SAO group uses a reference sector approach, assuming that the column in a reference sector over the Pacific Ocean is mainly of stratospheric origin, and subsequently assuming zonal invariance of stratospheric NO_2. To account for the small amount of tropospheric NO_2 over the Pacific, a correction is applied based on output from the GEOS-CHEM model (Bey et al., 2001) for the day of observation (Martin et al., 2002). The Bremen group uses stratospheric NO_2 fields from the SLIMCAT model (Chipperfield, 1999), scaled such that they are consistent with the GOME observations in the Pacific Ocean reference sector (Savage et al., 2004; Richter et al., 2005). As the tropospheric columns over this area are forced to zero, the columns from the Bremen retrieval are really "tropospheric excess columns". In the Dalhousie/SAO retrieval a correction is applied to account for the small amount of tropospheric NO_2 over the Pacific. KNMI has developed an assimilation approach in which the GOME slant columns force the stratospheric distribution of NO_2 of the TM4 model to be consistent with the observations (Boersma et al., 2004). The latter two approaches are introduced to account for the dynamical variability of the stratosphere. Especially in the winter this variability may be a dominant source of error over northern mid- and high latitudes in relatively clean areas. The Dalhousie/SAO retrieval does not provide data poleward of 50° S and 65° N due to concerns about stratospheric variability not accounted for in their retrieval.

3. Tropospheric air-mass factor: The tropospheric slant column has to be converted to a vertical column amount based on radiative transfer calculations. These cal-

culations depend sensitively on the accuracy of the cloud characterization, the surface albedo, the model profile shape, aerosols and temperature. The three independent radiative transfer codes used are LIDORT (Spurr et al., 2001; Spurr, 2002) (Dalhousie/SAO), SCIATRAN (Rozanov et al., 1997) (Bremen) and DAK (de Haan et al., 1987; Stammes et al., 1989) (BIRA/KNMI). The European retrievals use look-up tables to improve retrieval speed; the Dalhousie/SAO retrieval conducts a new radiative transfer calculation for every GOME observation.

The tropospheric air-mass factor calculation is based on the following ingredients:

1. Clouds: Clouds obscure the high NO_2 concentrations near the surface and are therefore a major potential source of error. Based on given uncertainties in cloud retrieval algorithms the estimated contribution to the precision of the tropospheric column is 15–30% in polluted areas (Martin et al., 2002; Boersma et al., 2004). The Dalhousie/SAO group uses GOMECAT cloud retrieval information (Kurosu et al., 1999) and treats clouds as Mie scatterers; the KNMI group uses cloud fraction and cloud top height from the Fast Retrieval Scheme for Cloud Observables (FRESCO) (Koelemeijer et al., 2001) and treats clouds as Lambertian surfaces. Both exclude scenes in which more than 50% of the backscattered intensity is from the cloudy sky fraction of the scene, corresponding to a cloud (or snow) cover of about 20%. The Bremen retrieval is performed only for nearly cloud-free pixels, with a FRESCO cloud fraction less than 20%. A difference between Bremen and the other groups is that the cloud is neglected for fractions less than 20%, while the other two retrievals explicitly account for the influence of the small cloud fractions on the radiative transfer.

2. Surface albedo: The sensitivity of the GOME instrument to near-surface NO_2 is very sensitive to the surface reflectivity near 440 nm. The quoted uncertainties in the surface reflectivity databases (Koelemeijer et al., 2003) translate into vertical NO_2 column uncertainties of about 15–35% in polluted areas (Martin et al., 2002; Boersma et al., 2004). The Bremen and Dalhousie/SAO retrievals are based on

the GOME surface reflectivities (Koelemeijer et al., 2003). The BIRA/KNMI retrieval is based on TOMS albedos (Herman and Celarier, 1997) which are wavelength corrected with the ratio of GOME reflectivities at 380 nm and 440 nm.

3. Profile shape: The sensitivity of GOME to NO_2 is altitude dependent, which implies that the conversion to vertical columns is dependent on the shape of the vertical NO_2 profile. (Due to the small optical thickness of NO_2 the retrieval is nearly independent of the a priori total tropospheric NO_2 column.) The use of one generic profile shape will lead to large errors in the total column estimate of up to 100%. The vertical profile is strongly time and space dependent, related to the distribution and strength of sources, the chemical lifetime and horizontal/vertical transport. This is the main motivation for using NO_2 profiles from chemistry transport models as first-guess input for the air-mass factor calculations. The Dalhousie/SAO and BIRA/KNMI retrievals use collocated daily profiles at overpass time from GEOS-CHEM and TM4, respectively; the Bremen retrieval uses monthly averages from a run of the MOZART-2 model for the year 1997. These models have similar resolutions between 2° and 3° longitude/latitude. The estimated precision of the tropospheric column related to profile shape errors is only 5–15% (Martin et al., 2002; Boersma et al., 2004). However, one may expect systematic differences among the models, for instance related to the description of the boundary layer and vertical mixing at the GOME overpass time. These systematic differences will lead to tropospheric column offsets among the three retrievals.

4. Aerosols: The Bremen and Dalhousie/SAO retrievals explicitly account for aerosols. The Bremen retrieval is based on three different aerosol scenarios (maritime, rural, and urban) taken from the LOWTRAN database. The selection of the aerosol type is based on sea-land maps and CO_2 emission levels. The Dalhousie/SAO retrieval uses collocated daily aerosol distributions at overpass time from the GEOS-CHEM model (Bey et al., 2001; Park et al., 2003, 2004).

The BIRA/KNMI retrieval does not explicitly account for aerosols, based on the argument that the aerosol impact on the retrieval is partly accounted for implicitly by the cloud retrieval algorithm.

5. Temperature: The neglect of the temperature dependence of the NO_2 cross section may lead to systematic errors in the tropospheric slant columns up to –20% (underestimating the column) (Boersma et al., 2004). A temperature correction is applied in the BIRA/KNMI and Dalhousie/SAO retrievals, but not in the Bremen retrieval reported here.

In polluted regions the retrieval uncertainty is dominated by the air-mass factor errors related to cloud properties, surface albedo, NO_2 profile shape and aerosols. The retrieval precision for individual observations is on the order of 35 to 60% (Boersma et al., 2004; Martin et al., 2002, 2003b). A substantial part of the error is systematic and will influence the monthly mean results. In relatively clean areas (columns less than 1×10^{15} molecules cm^{-2}) the retrieval error is dominated by the slant-column fitting noise (especially at low-latitudes) and the estimate of the stratospheric background (especially at higher latitudes in winter). The detection limit is around 5×10^{14} molecules cm^{-2}.

3 Model setup

The analysis presented in this paper is part of a large model intercomparison study on air quality and climate change coordinated by the European Union project ACCENT (Atmospheric Composition Change: the European NeTwork of excellence). Other aspects of this wider modeling study include an intercomparison of present-day and near-future global tropospheric ozone distributions, budgets and associated radiative forcings (Stevenson et al., 2006); a detailed analysis of surface ozone, including impacts on human health and vegetation (Ellingsen et al., 2006[2]); an analysis and validation of

[2]Ellingsen, K., van Dingenen, R., Dentener, F. J., et al.: Ozone air quality in 2030: a multi model assessment of risks for health and vegetation, J. Geophys. Res., in preparation, 2006.

nitrogen and sulfur deposition budgets (Dentener et al., 2006b); and a comparison of modeled and measured carbon monoxide (Shindell et al., 2006[3]).

The intercomparison study presented by Stevenson et al. (2006) comprises a large number of models in twenty-six different configurations. Out of these a subset of 17 models produced tropospheric NO_2 columns for comparison with GOME. An overview of the models is given in Table A2 of the Appendix. The Global Modelling Initiative (GMI) team delivered output from different simulations driven by three sets of meteorological data; the different configurations are counted here as separate models. Most of the models analyzed in this study are chemistry transport models (CTMs) driven by offline meteorological data. The chemistry climate models (CCMs) – GMI-CCM, GMI-GISS, IMPACT, NCAR, and ULAQ – are all atmosphere-only models and used prescribed sea surface temperatures (SSTs) valid for the 1990s. None of these was set up in fully coupled mode; the meteorology is thus not influenced by the chemical fields. The LMDz-INCA model was set up in CTM mode with winds and temperature relaxed towards ERA-40 reanalysis data from the European Centre for Medium-Range Weather Forecasts (ECMWF) for the year 2000.

Nearly all CTMs used assimilated meteorological data for the year 2000; only GMI-DAO used assimilated fields for March 1997–February 1998. Most models produced daily 10:30 local time or hourly output; MATCH-MPIC and IMAGES only provided monthly mean 10:30 local time data. For a proper comparison it is therefore useful to separate the models into two classes. The first (ensemble A) includes the CTMs that are driven by meteorology for the year 2000 and have provided daily (or hourly) data; the second (ensemble B) includes the CCMs and the GMI-DAO, MATCH-MPIC, and IMAGES CTMs. The nine A-ensemble models (CHASER, CTM2, FRSGC/UCI, GEOS-CHEM, LMDz-INCA, MOZ2-GFDL, p-TOMCAT, TM4, and TM5) attempt to reproduce the measurements on a day-by-day basis; from the B-ensemble models we

[3]Shindell, D. T., Faluvegi, G., Stevenson, D. S., Emmons, L. K., Lamarque, J.-F., Pétron, G., Dentener, F. J., Ellingsen, K., et al.: Multi-model simulations of carbon monoxide: Comparison with observations and projected near-future changes, J. Geophys. Res., submitted, 2006.

can only expect agreement in a time-averaged sense. The difference between the two ensembles will be clearly demonstrated when we discuss sampling issues in Sect. 5.3.

A description of the models' characteristics and of the setup of the intercomparison simulations with focus on various aspects important for tropospheric ozone is given by Stevenson et al. (2006). Here we will give a brief summary of the setup of the year-2000 simulations and treat some of the issues related to tropospheric NO_2 in more detail. With the exception of p-TOMCAT, all models included a reaction for the hydrolysis of N_2O_5 on aerosols (Dentener and Crutzen, 1993; Evans and Jacob, 2005). The reaction probability for this reaction varied between 0.01 and 0.1 (see Table A2).

Emissions of NO_x, carbon monoxide (CO), non-methane volatile organic compounds (NMVOCs), sulfur dioxide (SO_2), and ammonia (NH_3) were specified on a $1^\circ \times 1^\circ$ grid. To reduce the required spinup time of the near-future scenario simulations of the intercomparison study, the methane mixing ratios were specified throughout the model domain; for the year 2000 a global methane mixing ratio of 1760 ppbv was assumed. The anthropogenic emissions of the shorter-lived ozone precursor gases were based on national estimates from the International Institute for Applied Systems Analysis (IIASA) for the year 2000 (Cofala et al., 2005; Dentener et al., 2005), distributed according to the Emission Database for Global Atmospheric Research (EDGAR) version 3.2 for the year 1995 (Olivier and Berdowski, 2001). Emissions from international shipping were added by extrapolating the EDGAR3.2 emissions for 1995, assuming a growth rate of 1.5% per year. The resulting anthropogenic emissions were specified on a yearly basis, including separate source categories for agriculture (NH_3 only), industry, the domestic sector, and traffic. The corresponding emission totals for NO_x are given in Table 1. In some models (GMI, IMAGES, TM4, and TM5) the industrial emissions were released between 100–300 m above surface, using a recommended vertical profile; other models simply added emissions to their lowest layer. For aircraft NO_x emissions a total of 2.58 Tg NO_2 (0.79 Tg N) was recommended for the year 2000, with distributions from NASA (Isaksen et al., 1999) or ANCAT (Henderson et al., 1999).

Monthly emissions from biomass burning were specified based on the satellite-

derived carbon emission estimates from the Global Fire Emissions Database (GFED) version 1 (van der Werf et al., 2003) averaged over the years 1997–2002, in combination with ecosystem dependent emission factors from Andreae and Merlet (2001). The corresponding yearly total NO_x emissions are given in Table 2. The main reason for using the 1997–2002 average emissions is that the year-2000 simulations analyzed in this study served as the reference for the scenario simulations of the wider intercomparison study on air quality and climate change. To evaluate the impact of interannual variability in the emissions from biomass burning, we performed an additional simulation with the TM4 model using the GFED emissions for the year 2000 (see Sect. 5). Height profiles were specified for biomass burning emissions to account for fire-induced convection, based on a suggestion by D. Lavoué (personal communication, 2004). These profiles were implemented by a subset of models (GMI, IMAGES, IMPACT, MOZ2-GFDL, TM4, and TM5). In these models the emissions from biomass burning were distributed over six layers from 0–100 m, 100–500 m, 500 m–1 km, 1–2 km, 2–3 km, and 3–6 km. The biomass burning emissions are further described by Dentener et al. (2006c).

Recommendations were given for the natural emissions of trace gases (Stevenson et al., 2006). For the NO_x emissions from soils, which represent natural sources augmented by the use of fertilizers, the models used values between 5.5 and 8.0 Tg N/yr. Another important but relatively uncertain source is the NO_x production by lightning (see Boersma et al., 2005; and references therein), which varied between 3.0 and 7.0 Tg N/yr (see Table A2).

4 Method of comparison

In order to systematically compare models and retrievals, the model NO_2 fields were analyzed at 10:30 local time and collocated with the GOME measurements. This was done following the sampling of the BIRA/KNMI and Dalhousie/SAO retrievals, which include only forward-scan scenes with a cloud radiance fraction lower than 0.5 for solar zenith angles smaller than 80°. The retrieval by the Bremen group uses a slightly

different selection based on a cloud fraction threshold of 20%. These differences imply that some inconsistencies remain in the comparison of models with the Bremen retrieval. Nevertheless, our collocation procedure corrects for most of the sampling bias of the retrievals resulting from incomplete spatial and temporal coverage of the satellite observations.

For the selected scenes, the modeled (sub)column density fields were linearly interpolated to the centre of the GOME ground pixels. As an intermediate step the data were mapped onto a resolution of 0.5°×0.5°. The forward scans cover an area of 320 km×40 km; the horizontal resolution of the models, on the other hand, ranges from 1°×1° (TM5 over zoom regions) to 22.5°×10° (ULAQ), but is typically between 2° and 5° longitude/latitude. To eliminate the effect of such resolution differences among the models and between models and retrievals, the model as well as the retrieval data were smoothed to 5°×5° using a moving average.

The impact of collocating the model data with the observations is assessed by comparing the tropospheric NO_2 columns from sampled and unsampled model output. (In the latter case the 10:30 local time column densities were mapped directly onto a resolution of 0.5°×0.5° and thereafter smoothed to 5°×5°.) In fact, by comparing the sampled and unsampled model output, we can actually estimate the sampling biases in the monthly or yearly retrieval maps.

Such sampling biases are caused by temporal correlations between the local cloud cover and the NO_2 column density. In the annual mean this bias is to large extent determined by seasonal variations, for instance in regions dominated by emissions from biomass burning. This seasonal contribution to the sampling bias can easily be removed by constructing a "corrected" annual mean by first calculating the monthly means and then averaging the monthly means. What remains is the contribution to the sampling bias resulting from day-to-day variability. To estimate this contribution, we removed the day-to-day variability in the 10:30 local time column output from the models by taking the monthly mean before sampling the data. The contribution from day-to-day variability to the sampling bias follows as the difference between the sampled daily and

the sampled monthly fields.

In summary, the total sampling bias (SB_{total}) in the tropospheric NO_2 column density is given by

$$SB_{total} = \overline{\mathbf{S}(TCD(n))} - \overline{TCD(n)},$$

where TCD(n) is the 10:30 local time tropospheric column density field on day n, the sampling operator **S** selects the scenes that have actually been retrieved, and the overbar denotes a time averaging, per month or per year. The contribution from day-to-day variability to the sampling bias ($SB_{day-to-day}$) can then be expressed as

$$SB_{day-to-day} = \overline{\mathbf{S}(TCD(n))} - \overline{\mathbf{S}(\mathbf{M}(TCD(n)))},$$

where the operator **M** assigns the monthly mean values to the daily fields. The remaining contribution related to seasonal variations ($SB_{seasonal}$) is thus given by the difference between the sampled monthly fields and unsampled (monthly) fields:

$$SB_{seasonal} = \overline{\mathbf{S}(\mathbf{M}(TCD(n)))} - \overline{TCD(n)} = \overline{\mathbf{S}(\mathbf{M}(TCD(n)))} - \overline{\mathbf{M}(TCD(n))},$$

which vanishes in the monthly means, but is nonzero in the annual mean.

The corresponding expressions for the annual mean and the corrected annual mean tropospheric NO_2 column density are as follows:

$$\text{annual mean} = \overline{\mathbf{S}(TCD(n))}^{annual}$$

$$\text{corrected annual mean} = \left\langle \overline{\mathbf{S}(TCD(n))}^{monthly} \right\rangle_{annual}.$$

Here the overbar denotes the annual or monthly average and the brackets denote an averaging over the separate months weighted by the total number of days per month. Unless stated otherwise, the annual means presented in this study therefore always correspond to the unweighted averages over the individual scenes retrieved throughout the year.

Most models provided tropospheric NO_2 columns as two-dimensional (2-D) fields assuming for the tropopause the level where the ozone mixing ratio equals 150 ppbv, as is done in the study by Stevenson et al. (2006). As the contributions from the upper troposphere and lower stratosphere are negligibly small compared to those from the lower and middle troposphere over polluted regions, the tropospheric NO_2 column density field is relatively insensitive to the exact tropopause definition. Based on the 3-D 10:30 local time NO_2 fields from the TM4 model, we estimate that the assumption of a constant tropopause pressure of 200 hPa would change the annual mean tropospheric NO_2 column density by an amount between –0.05 10^{15} molecules cm^{-2} over tropical and subtropical continental regions and $+0.1\times10^{15}$ molecules cm^{-2} at high latitudes.

Other models, including the three GMI models, LMDz-INCA and p-TOMCAT, also provided 3-D NO_2 fields at 10:30 local time. The availability of 3-D model output allows for a more direct comparison with the retrievals after convolution of the modeled tropospheric NO_2 profiles with the averaging kernels of the retrievals. Application of averaging kernels makes the comparison independent of retrieval errors resulting from a priori profile assumptions (Eskes and Boersma, 2003). In this study the averaging kernels were taken from the BIRA/KNMI retrieval. The convolution was performed at the vertical resolution of the averaging kernels, having 35 layers in the vertical; 10:30 local time surface pressure fields from the European Centre for Medium Range Weather Forecasts (ECMWF) were used to regrid the model subcolumns in the vertical (see Sect. 5.4).

5 Results

5.1 Global maps for retrievals and models

In Fig. 1 we present the annual mean NO_2 columns from the three retrievals for the year 2000. Shown are the original retrieval data mapped to a resolution of $0.5^\circ\times0.5^\circ$ as well as, for comparison with models, smoothed to $5^\circ\times5^\circ$. The retrievals show quali-

tatively similar patterns of pollution. Large-scale pollution is most pronounced over the eastern United States, Europe, and eastern China. High tropospheric NO_2 columns are also clearly observed over California, South Korea, and Japan, as well as over the industrial Highveld region of South Africa. Enhanced levels of pollution are further seen over the Indian subcontinent, especially over the Ganges valley in the north, around Delhi and Calcutta; over the Middle East, in particular around the main ports of the Persian Gulf, around the Red Sea port of Jedda near Mecca, and around the cities of Riyadh, Cairo and Tehran; over the metropolitan cities of Mexico City, São Paolo/Rio de Janeiro, Buenos Aires, Moscow, Ekaterinburg, Chongqing (Central China), Hong Kong, and Sydney. Relatively high tropospheric NO_2 columns are also observed over the savanna regions of Northern Africa south of the Sahara and Central Africa south of the Equator; over the savanna, grassland and seasonally dry forest regions of South America; and further over parts of Southeast Asia (Burma, Thailand, Malaysia and the islands Sumatra and Java of the Indonesian archipelago). Relatively low values are observed over the oceans, over desert regions and other remote areas. These features are common to all three retrievals and remain discernible after smoothing to $5^\circ\times5^\circ$.

The corresponding maps for the individual models of ensemble A and B are presented in Figs. 2 and 3, respectively. Shown are the 10:30 local time model output fields collocated with the measurements and smoothed to $5^\circ\times5^\circ$. The large-scale patterns observed in the retrievals are reproduced in a qualitative sense by the models. More localized pollution around main ports and metropolitan cities is at best partially resolved and is visible only in the higher-resolution models.

The spatial correlations between the annual mean tropospheric NO_2 column density field of the individual models and retrievals are given in Table 3. It demonstrates that the smoothing to $5^\circ\times5^\circ$ systematically improves the correlations between models and retrievals, suggesting that the models do not accurately reproduce the small-scale features of the retrievals. Table 3 also shows that, even after smoothing, the observed patterns are better reproduced by the higher-resolution chemistry transport models of ensemble A than by the relatively coarse models of ensemble B. In particular the ULAQ

model has difficulty representing the spatial distribution of the NO_2 column density, due to its coarse resolution of 22.5°×10°.

The differences in model performance are caused by a complex interplay of various aspects of the chemistry and dynamics of the models. A comprehensive analysis of these factors is beyond the scope of this paper, but some of the differences can be explained in terms of differences in OH levels, N_2O_5 hydrolysis rates, and vertical mixing.

As estimated by Stevenson et al. (2006), the atmospheric CH_4 lifetime in the models varies between 7.18 and 12.46 years (see Table A2). As the major sink of CH_4 is oxidation by OH, this indicates that there are rather large differences in OH among the models. Thus, the relatively low tropospheric NO_2 columns of the IMPACT, GMI-CCM and GMI-DAO models might be explained if we assume that the NO_x lifetime in these models is reduced due to relatively high levels of OH, corresponding to a relatively low lifetime of CH_4. Similarly, the relatively high CH_4 lifetime in CTM2 is consistent with the relatively high columns simulated by this model.

Other important factors determining the lifetime of NO_x are the reaction probability for hydrolysis of N_2O_5 and the description of the different types of aerosols. The models analyzed here typically include the hydrolysis reaction on sulfate aerosols with a reaction probability in the range 0.04–0.1 (see Table A2). Evans and Jacob (2005) recently proposed a new parametrization for the reaction probability as a function of the local aerosol composition, temperature and relative humidity. This parametrization is included in the GEOS-CHEM model. The updated reaction probability has a global mean value of 0.02 and increases the tropospheric NO_x burden by 7%, compared to a simulation in which a uniform value of 0.1 is assumed. The largest increases were found in winter, up to 50% at subtropical latitudes.

Vertical mixing is important mainly for two competing reasons. On the one hand, the lifetime of NO_x increases with height. In summer it varies between several hours to a day in the lower troposphere and several days to a week in the upper troposphere. On the other hand, the daytime NO_2/NO ratio typically decreases by an order of magnitude

from the surface to the upper troposphere, mainly because the reaction $NO+O_3 \rightarrow NO_2$ progresses more slowly at lower temperatures. For explaining the differences in tropospheric NO_2 columns, the changes in the partitioning between NO_2 and NO seem to be more important than the changes in the lifetime of NO_x. For instance, it has been reported that the venting out of the boundary layer is too vigorous in LMDz-INCA (Hauglustaine et al., 2004) (see also Sect. 5.4), which is consistent with the relatively low tropospheric NO_2 columns simulated with this model. In contrast, the NCAR and MOZ2-GFDL models, which produce relatively high NO_2 columns, use a boundary layer mixing scheme that tends to confine pollutants relatively strongly (Horowitz et al., 2003).

The NO_2 levels in the NCAR model may also be too high because the conversion of organic nitrates and isoprene nitrates to NO_2 is too efficient. Other aspects of the chemical and dynamical schemes as well as differences in deposition rates and natural emissions (see Table A2) may also be relevant.

5.2 Mean performance and uncertainties

Figure 4 displays the ensemble averages and the corresponding standard deviations for the three retrievals, for the full model ensemble, and for model ensemble A. For a proper comparison the 10:30 local time model output was collocated with the measurements, as was done in Figs. 2 and 3. Moreover, retrieval and model averages and standard deviations were calculated after smoothing the data to 5°×5°. The three retrievals give significantly different NO_2 columns over the continental source regions. Over the eastern United States and over eastern China the standard deviation among the retrievals goes up to about 1.5 and 2.0×10^{15} molecules cm^{-2}, respectively. Larger differences are observed over South Africa and Europe, where the standard deviation approaches 2.5 and 3.0×10^{15} molecules cm^{-2}, respectively. Except for the Highveld region of South Africa, the major industrial regions are much less polluted in the Dalhousie/SAO retrieval than in the BIRA/KNMI and Bremen retrievals (see Fig. 1). For the model ensemble we find comparable standard deviations over the eastern United

States, Europe and eastern China – up to 2.0×10^{15} molecules cm^{-2} for the full ensemble and up to 1.5×10^{15} molecules cm^{-2} for ensemble A. Over India and northeastern Australia the models also show a smaller spread than the retrievals; the reverse is observed over Central Africa south of the Equator.

Note that the standard deviation among the A-ensemble models is generally significantly smaller than for the full model ensemble. The ensemble averages on the other hand are very similar, indicating that the use of climate models introduced random errors. This similarity is demonstrated more clearly in Fig. 5, which shows the difference between the model ensemble averages and the retrieval average. The full ensemble produces a more diffuse pattern than the restricted A ensemble, resulting in slightly higher values over oceans and remote regions; over polluted regions, the two ensembles give nearly identical average values. On average the models underestimate the retrievals in industrial regions and overestimate the retrievals in regions dominated by biomass burning. By far the strongest underestimation of up to 6.0×10^{15} molecules cm^{-2} is found over the Bejing area of eastern China. Over the Highveld region of South Africa as well over Western Europe south of Scandinavia the models underestimate the retrievals by up to 4.0×10^{15} molecules cm^{-2}. Smaller underestimations are found over the other industrial regions mentioned in Sect. 5.1, in particular over the eastern United States, California, the Persian Gulf, India, Hong Kong, South Korea and Japan. The models are also unable to reproduce the relatively high NO_2 columns over the southwest of Canada. The strongest overestimations (up to 1.5×10^{15} molecules cm^{-2}) are found over the savanna regions of Brazil south of the Amazon basin and over Angola. The models further overestimate the retrievals over Zambia and the southern Congo, over the south coast of West Africa, over the Central African Republic and southern Sudan, as well as over Southeast Asia. Simulated columns are also higher than retrieved over the North Atlantic, Ireland, Scotland, Scandinavia and the Baltic States.

5.3 Sampling bias

Figure 6 shows the annual mean bias distribution resulting from incomplete spatial and temporal coverage of the GOME measurements, as estimated from the models. As a proxy for the actual sampling bias of the retrievals, we have calculated the difference between the sampled and unsampled 10:30 local time output from the models. The best estimate of the sampling bias is derived on the basis of the A-ensemble; the corresponding result for the B-ensemble models can only account for part of the actual sampling bias, as will be demonstrated below.

Both ensembles consistently indicate that the satellite products are positively biased over the large biomass burning regions of Africa (up to 48%), South America (up to 38%), and parts of Southeast Asia, including Burma, Laos and Thailand (up to 28%). The sampling biases over these regions are related to the fact that there are relatively few observations during the wet seasons due to the presence of clouds; the annual means are therefore biased towards the high column values observed during the dry burning season. Relatively small positive biases are found over the north of Canada, over northern Kazakhstan, and over eastern Siberia. Because of the similarity of the bias patterns generated by the two ensembles, these biases must also be caused by correlations on seasonal time scales between local cloud or snow cover and tropospheric NO_2 column density.

Negative biases are observed over the eastern United States, Europe, and eastern China. In these regions, the two ensembles give rather different results, however. Our best estimates based on the A-ensemble models indicate negative biases down to -1.7×10^{15} molecules cm^{-2} (–47%) over Europe, -1.5×10^{15} molecules cm^{-2} (–34%) over the eastern United States, and -0.8×10^{15} molecules cm^{-2} (–21%) over eastern China. The B-ensemble models would result in significantly smaller bias estimates in these regions, because the tropospheric NO_2 columns from these models do not reflect the synoptic-scale meteorological variability of the year 2000. The ensemble-A models, on the other hand, do account for day-to-day fluctuations related to meteorological

conditions. The contribution of day-to-day variability to the sampling was calculated as described in Sect. 4. Figure 7 shows that this contribution is very different for the two sets of models. For the B-ensemble models we find a negligible contribution from day-to-day correlations (time scales shorter than a month); for this set of models the sampling biases shown in Fig. 6 are therefore almost entirely related to correlations on seasonal time scales. This is not the case for the A-ensemble models, where day-to-day correlations do give rise to an additional contribution to the sampling bias. In fact, the day-to-day sampling bias is as large -1.0×10^{15} molecules cm^{-2} over the eastern United States and in the range –0.7 to $+0.4\times10^{15}$ molecules cm^{-2} over eastern China, and accounts for most of the sampling bias over these regions. There is also a significant impact over Europe, where negative contributions down to -0.9×10^{15} molecules cm^{-2} are found over Scandinavia and Central Europe and positive contributions up to 0.5×10^{15} molecules cm^{-2} over Western Europe.

It should be emphasized that these numbers are estimates based on model assumptions and that in reality a different bias could exist. The impact of clouds, for example, could be quite different depending on the vertical profile of NO_2, which in turn depends on the vertical mixing and vertical emission profile used in the models.

Note also that our definition of the sampling bias does not account for differences between the 10:30 local time and the 24-h average tropospheric NO_2 column density. From a simulation of the TM4 model with diurnally varying anthropogenic emissions in Europe (see Sect. 6.2), we estimate that the 10:30 local time columns over this region are 71.7% (February) to 55.9% (October) – or 65.6% in the corrected annual mean – of the corresponding diurnal average values. Similar ratios were reported by Velders et al. (2001). For the comparison with NO_2 retrievals from space it is therefore essential to consider only model output at or close to the overpass time of the satellite.

5.4 Averaging kernels

The results presented above have all been obtained on the basis of the 2-D output fields from the model. In this section we will test the sensitivity of the results to the

application of averaging kernels. Three models from ensemble A provided 10:30 local time 3-D NO_2 fields: LMDz-INCA, p-TOMCAT and TM4. In Fig. 8 we present for these models the tropospheric column density maps obtained by convolution of the collocated data with the averaging kernels of the BIRA/KNMI retrieval, together with the difference with the corresponding maps derived from the 2-D model output fields (shown earlier in Fig. 2). LMDz-INCA and p-TOMCAT show similar patterns of sensitivity over industrial regions. For these models the application of the averaging kernels leads to an increase of up to 1.5×10^{15} molecules cm^{-2} over eastern China and up to 1.0×10^{15} molecules cm^{-2} over the northeastern United States and over Europe. These increases imply that the vertical tropospheric NO_2 profile in these regions is not as steeply decreasing with height in the LMDz-INCA and p-TOMCAT models as does the a priori profile assumed in the BIRA/KNMI retrieval.

TM4 shows a much less sensitive response in these regions, which can be understood from the fact that the a priori profile used in the BIRA/KNMI retrieval is actually based on the TM4 model. Nevertheless the application of the averaging kernels does have a nonzero impact in large parts of the world even for the TM4 model. This is related to the fact the retrieval has used another version of the model with different emissions from anthropogenic sources and from biomass burning; moreover, in the current version of the model the biomass burning emissions are also distributed as a function of height, as described in Sect. 3. Indeed the TM4 model is most sensitive to the application of the averaging kernels over the biomass burning regions of Africa. Here the response pattern is similar for the three models with increases of over southern Sudan, the Central African Republic and the southern Congo, and decreases over Angola and Zambia, as well as over the south coast of West Africa.

Increases are found where the model profile is flatter than the a priori profile and can be explained by the height distribution of the biomass burning emissions in the TM4 model simulation; decreases are related to differences between the Global Fire Emissions Database (GFED) emissions assumed in this intercomparison study and the biomass burning emission inventory assumed in the TM4 model version used in

the retrieval (estimates for the year 1997 from the European Union project POET). To demonstrate the validity of this argument, we performed an additional simulation with the TM4 model following the setup of Sect. 3, but with all emissions from biomass burning released near the surface (below 100 m). Over the biomass burning regions the response to the application of the averaging kernels changes in line with the explanation given above: with biomass burning emissions released near the surface, the regions of positive impact in Africa have disappeared and the regions of negative impact have extended significantly (Fig. 8).

The application of the averaging kernels yields a closer agreement between the LMDz-INCA and p-TOMCAT models with the BIRA/KNMI retrieval over the large parts of the industrialized world. However, averaging kernels are at best part of the explanation for the observed discrepancy between models and retrievals: the inclusion of profile information from the models removes only a fraction of the underestimation by the models of the retrieved columns over industrial regions and may even lead to enhanced discrepancies over some of the biomass burning regions. Since the response is determined by local differences between the a priori profile assumed in the retrieval and the corresponding profile from the model, details of the response pattern may be quite different for the other models. Moreover, it should be realized that the averaging kernels used in this study allow for a more direct comparison with the BIRA/KNMI retrieval only.

5.5 Regional analysis

The seasonal cycle in tropospheric NO_2 from models and retrievals was analyzed in more detail for eight continental regions of relatively high pollution (see Fig. 9). These include industrial regions (the eastern United States, Europe, eastern China and South Africa) as well as the regions dominated by emissions from biomass burning (Northern Africa, Central Africa, South America and Southeast Asia). For these regions we calculated the monthly and yearly average tropospheric NO_2 column densities from the retrievals and from the collocated 10:30 local time model output, thus focusing

on differences not related to sampling issues. In Fig. 10 the seasonal cycle obtained with the A-ensemble models is compared with the retrievals. The left panel shows the monthly mean values derived from the 2-D model output; the right panel shows the corresponding values obtained by application of the averaging kernels to the 3-D output from LMDz-INCA, p-TOMCAT and TM4, together with the retrieved monthly means.

As shown previously, over the industrial regions the spread in absolute column abundances is generally larger among the retrievals than among the A-ensemble models (see Fig. 4) and on average the models tend to underestimate the retrieved values (see Fig. 5). From the seasonal cycles shown in Fig. 10, it can be observed the differences among the retrievals are particularly pronounced in wintertime; moreover, it can be seen that the ensemble average discrepancy between models and retrievals is dominated by the fact that the models do not reproduce the highest wintertime values produced by the retrievals.

Following the argument of Sect. 5.1, this might indicate that many of the boundary layer schemes used in the models have difficulty suppressing the vertical mixing under stable conditions. Possibly the models also tend to overestimate the N_2O_5 hydrolysis reaction rate. According to Evans and Jacob (2005), the assumption of a uniform reaction probability of 0.1 would lead to an underestimation of the NO_x concentrations by up to 50% in wintertime. However, even the models with lower reaction probabilities as well as the GEOS-CHEM model, in which the parametrization of Evans and Jacob (2005) is applied, are unable to reproduce the strong wintertime enhancement seen in the European retrievals over industrial regions.

The discrepancy between models and retrievals is particularly pronounced over eastern China. The most likely explanation is that the IIASA/EDGAR3.2 inventory significantly underestimates the emissions from eastern China, especially in wintertime. Kunhikrishnan et al. (2004a) performed simulations with the MATCH-MPIC model using anthropogenic emissions from EDGAR version 2.0 and also underestimated tropospheric NO_2 over eastern China in winter compared to GOME columns retrieved by the Bremen group. A growing body of evidence suggests that the anthropogenic emis-

sions from eastern China are significantly higher than generally assumed. Caveats in bottom-up inventories for China were reported in several recent publications. Large discrepancies were found between bottom-up estimates of CO emissions from fossil fuel and biofuel use and top-down estimates based on CO retrievals from the MOPITT instrument for the year 2000 (Arellano et al., 2004; Pétron et al., 2004). Wang et al. (2004) used aircraft observations over the northwestern Pacific and measurements from two Chinese ground stations during the spring of 2001 to constrain estimates of NO_x emissions from China. Their inversion analysis required an increase of 47% in the Chinese emissions compared to the a priori estimates from the bottom-up inventory by Streets et al. (2003). According to Wang et al. (2004), the large increase inferred for the central part of eastern China could not be accommodated by any reasonable adjustment in sources from combustion of either fossil or biofuel; instead they proposed that the missing source of NO_x may be associated with microbial decomposition of organic waste and with intensive use of chemical fertilizer.

Over the Highveld region of South Africa we find a strong discrepancy between models and retrievals throughout the year, suggesting that the regional emissions used in the models are more than a factor of 2 too low. Summertime NO_2 columns also seem to be underestimated over the eastern United States; the relatively large spread among the retrievals over Europe prevents us from drawing any more definite conclusions for this region.

Part of the discrepancies between models and retrievals is related to the assumption that the anthropogenic emissions are constant throughout the year. Streets et al. (2003) examined the potential seasonality of Chinese NO_x emissions due to heating in homes, assuming a dependence of stove operation on outdoor temperature, and estimated a 20% difference between maximum and minimum emissions from fuel combustion. Martin et al. (2003b) analyzed the seasonality in NO_x emissions by optimizing monthly emission estimates using a combination of GOME tropospheric NO_2 observations and model calculations. To first order approximation the monthly top-down emission estimates are found by local scaling of the a priori emissions with the

ratio between the retrieved and the modeled NO_2 columns (Martin et al., 2003b). This approach was followed in the inversion study by Jaeglé et al. (2005), who used output from the GEOS-CHEM model and a previous version of the Dalhousie/SAO retrieval to derive optimized estimates of NO_x emissions for the year 2000 and partitioned the sources among fuel combustion (fossil fuel and biofuel), biomass burning and soils. The a posteriori emissions from fuel combustion were found to be aseasonal over most regions with the exception of Europe and East Asia, where the a posteriori emission estimates are 30–40% higher in winter than in summer.

Our results indicate that the top-down and a posteriori emission estimates derived from such inversion studies are very sensitive to the selected model and retrieval. Over the eastern United States, for instance, the retrievals from Bremen and BIRA/KNMI show a stronger seasonality than observed in the Dalhousie/SAO retrieval. Thus the conclusion by Jaeglé et al. (2005) that the NO_x emissions from fuel combustion in the United States for the year 2000 are aseasonal seems inconsistent with the European retrievals. These emissions are also aseasonal in the National Emissions Inventory for 1999 (NEI99) from the United States Environmental Protection Agency (EPA).

For the regions dominated by emissions from biomass burning, the timing of the seasonal cycle as observed in the retrievals is generally well reproduced by the models. Tropospheric NO_2 amounts over Northern Africa, South America and Southeast Asia reach their maxima simultaneously in models and retrievals; over Central Africa south of the Equator the peak value in the models occurs in July, whereas it is observed in the retrievals during August–September. For this region the models also show a relatively large spread in column amounts during the dry season. Systematic differences over the biomass burning regions can also be observed among the retrievals; the BIRA/KNMI product generally gives the highest values, the Bremen retrieval the lowest.

Nevertheless, it can be observed that the seasonal cycles over the African regions and over South America are significantly stronger in the models than in the retrievals. For Northern and Central Africa this is at least partly due to an underestimation of the retrieved tropospheric NO_2 columns by the models during the wet season. This

suggests that the NO_x emissions from soils are higher than assumed in the models, in support of the conclusions of Jaeglé et al. (2004, 2005). For South America on the other hand the models tend to overestimate the columns during the active dry season. Over Southeast Asia the models on average produce higher column values than the retrievals (see Fig. 5). However, throughout the year significantly more pollution is seen over Thailand in the BIRA/KNMI product than in the other two retrievals; with a few exceptions the models fall within the range of the retrievals for this region. It will be investigated in the next section to what extent these findings are influenced by the fact that biomass burning emissions for the years 1997–2002 instead of specific for the year 2000 were used in the models.

Regional results for the full model ensemble are presented in Fig. 11. It shows the yearly mean together with the minimum and maximum monthly mean values for models and retrievals. The full ensemble shows clearly more spread among individual models compared to the restricted ensemble A, especially over the industrial regions of the eastern United States, Europe, and eastern China as well as over Northern Africa. The difference between the models and retrievals over industrial regions is smallest for the Dalhousie/SAO retrieval. An overview of the corresponding ensemble means and standard deviations of the annual average NO_2 amount for the different regions is given in Table 4.

The yearly mean values of Fig. 11 and Table 4 are biased because of the incomplete coverage of the GOME measurements. As explained in Sect. 4, the contribution of seasonal correlations to the sampling bias can be removed by constructing a corrected annual mean from the monthly means weighted with the number of days per month. The resulting corrected annual mean tropospheric NO_2 column densities for the different regions are presented in Table 5 for models and retrievals. Under the assumption that the a priori emissions assumed in the models have a realistic seasonal cycle, these numbers would actually be the starting point for deriving top-down estimates of emissions. A more quantitative inversion should be based on the corresponding monthly values, shown in Fig. 10. Considering the relatively large spread in results, especially

among the current state-of-the-art retrievals, we have not attempted to perform such an inversion at this stage.

6 Sensitivity studies

6.1 Biomass burning emissions

The model results presented so far have been obtained on the basis of the average GFED biomass burning emissions for the years 1997–2002. To evaluate how this has affected the model results, we have performed an additional simulation with the TM4 model using the GFED emissions for the year 2000 (see Table 2). As shown in Fig. 12, the most significant effect of using the year-2000 emissions is to decrease the tropospheric NO_2 column density over the biomass burning regions south of the Amazon River, by up to 1.0×10^{15} molecules cm^{-2} over an extensive area of Central Brazil. Smaller decreases are found over parts of Southeast Asia, including the regions around Burma and Thailand as well as the Indonesian islands of Borneo and Sumatra. Here the 1997–2002 average emissions are clearly affected by the widespread forest fires observed during the 1997–1998 El Niño (van der Werf et al., 2004). Interannual variability of emissions seems relatively unimportant for Africa; using the year-2000 emissions here results in relatively small increases over Northern Africa and slightly reduces the tropospheric NO_2 columns over parts of Southern Africa. We also find a clear positive signal over the state of Montana in the northwest of the United States, where anomalously large forest fires occurred in 2000; this region cannot be clearly identified in the retrievals however.

Another possible explanation for some of the discrepancies between models and retrievals is related to uncertainties in the emission factors used for estimating the NO_x emissions from the GFED carbon emissions. The trace gas emission data used in the intercomparison study were based on the ecosystem dependent emission factors from Andreae and Merlet (2001). New values were recently proposed by Andreae (personal

communication, 2004). Most significant change is a reduction of emission factors for savanna regions, for NO_x by 39.7% (from 3.9 to 2.35); for tropical forests the NO_x emission factor has been slightly increased by 15.6% (from 1.6 to 1.85), while the value for extratropical forests remains unchanged (equal to 3.0). To test the sensitivity of the model results to the chosen emission factors, we performed an additional simulation with the TM4 model using the GFED emissions for the year 2000 in combination with the updated emission factors (see Table 2). The corresponding maps are presented in Fig. 13. Overall the updated emission factors give significantly lower levels of pollution from biomass burning. The pattern of biomass burning over South America seems to be improved, although significant discrepancies with the retrievals remain (see the correlations coefficients in Table 6).

A more detailed comparison of the different sensitivity studies is shown in Fig. 14 for the regions affected by emissions from biomass burning. It can be observed that the year-2000 emissions bring the TM4 model results for South America within the range of the retrievals. Given the close-to-average performance of TM4 in this region, it may be concluded that the overprediction of the retrievals by the models, which was observed in Fig. 10, is caused by the fact that average emission inventory for the years 1997–2002 were used. The results for the African biomass burning regions on the other hand are not significantly affected by this choice. In this respect our conclusions for Northern and Central Africa that the models underestimate the pollution during the wet season and overestimate the seasonal cycle are robust. It can be seen in Fig. 14 that the amplitude of the seasonal cycle in these regions is actually better represented, i.e., closer to the retrievals, using emissions estimates based on the updated emission factors. The discrepancies among the retrievals prevent us from drawing more definite conclusions on the validity of the updated emission factors compared to the old values. This is particularly so for Southeast Asia, where the results from the different sensitivity studies are all within the range of the retrievals.

6.2 Diurnal cycle in anthropogenic emissions

In the simulations presented so far the anthropogenic emissions were assumed to be time independent. We have seen in Sect. 5.5 that the comparison between models and the European retrievals over industrial regions suggests that anthropogenic NO_x emissions are higher in winter than in summer. In fact, to first order approximation (Martin et al., 2003b) the seasonal cycle in these emissions can straightforwardly be estimated as the ratio between the retrieved and modeled monthly column densities over industrial regions. A more detailed approach is needed to assess the impact of emission variations on time scales on the order of the NO_x lifetime. We have therefore performed an additional sensitivity simulation with the TM4 model to estimate the importance of diurnal variations in the anthropogenic emissions.

In this simulation we varied the emissions on an hourly basis in the European region defined above, according to specifications of the EDGAR database (available from http://www.mnp.nl/edgar). Although the temporal variations given there are provisional and need further validation, they are sufficiently accurate for our purpose. The set of temporal factors is based primarily on Western European data and was compiled for various anthropogenic source categories, including separate categories for traffic, industry, and the power and domestic sectors. As the power and industrial sectors were combined as a single source category in the emission input data for the model intercomparison, the corresponding diurnal cycle for the "industrial" emissions of this category was constructed by equal weighting of the temporal factors for the separate categories. For the region of interest this is a reasonable assumption, especially since the power and industrial sectors show a rather similar diurnal cycle. The resulting hourly factors for the three source categories describing emissions from traffic, industry and the domestic sector were implemented in the model by mapping the four European time zones onto a $1^\circ \times 1^\circ$ grid, taking into account the difference between summer time (daylight saving time) and winter time. Weekly and seasonal variations in anthropogenic emissions were neglected.

In Fig. 15 we compare the resulting seasonal cycle in the tropospheric NO_2 over Europe with the reference simulation and the retrievals. The impact of the diurnal variations in the emissions is to reduce the monthly simulated columns by 2.5% (July) to 4.1% (January), and by 3.2% averaged over the year. These numbers agree with a simple calculation in which horizontal transport is neglected and the NO_x lifetime τ is assumed to be constant. The NO_2 column at time t can then be expressed as

$$NO_2\,\text{column} = r(t) \cdot \int_0^\infty E(t-\Delta t)\exp(-\Delta t/\tau)\Delta t,$$

where $E(t)$ denotes the time-dependent emissions in the region of interest. The time-dependent prefactor $r(t)$ describes the fraction of NO_x molecules that are NO_2 in the column. In our approximation $r(t)$ is not affected by variations in emissions. We evaluated the integral for the different anthropogenic source categories as a function of the NO_x lifetime. Time t was set equal to 10:30 local time. For simplicity we here made the further assumption that the hourly factors define the diurnal cycle with respect to local time. The impact of diurnal variations follows by taking the ratio with the constant emissions case. Figure 16 shows the resulting ratio for the separate source categories, as well as for the combined anthropogenic emissions in Europe – the NO_x emissions from other sources were neglected in this calculation.

Based on this simple model calculation, for lifetimes shorter than 6 h we would expect the diurnal variations to give rise to enhanced tropospheric NO_2 columns over Europe at GOME overpass time. The TM4 model sensitivity study on the other hand shows only negative impacts. Indeed the TM4 model estimates agree with the simple model estimates for a lifetime between 8 and 32 h; the July value of 2.5% corresponds to a lifetime of 8 h. Strikingly, the maximum negative impact is about the same in both models (4.1% resp. 4.0%). The assumption of a constant lifetime breaks down at short lifetimes, when differences between day and night chemistry become important; we therefore expect the model to become more accurate at longer lifetimes.

In any case these calculations have convincingly demonstrated that the tropospheric NO_2 columns at 10:30 local time are only marginally affected by diurnal variations in anthropogenic emissions. By assuming constant emissions in the intercomparison study, the models have overestimated the columns over industrial regions by only a few percent.

7 Conclusions and discussion

As part of a wider model intercomparison assessing near-future air quality and couplings with climate change (Dentener, 2006a; Stevenson et al., 2006), this study compared tropospheric NO_2 from a large ensemble of atmospheric chemistry models with three state-of-the-art retrievals from the GOME satellite instrument for the year 2000. Output from 17 models, including offline chemistry transport models (CTMs) as well as chemistry climate models (CCMs), was collected at 10:30 local time, close to the overpass time of the satellite.

The synchronization of model output and observations is essential since the tropospheric NO_2 columns at 10:30 local time are significantly lower than the corresponding diurnal average values. We further demonstrated the importance of collocating the local time model data with the satellite measurements, to account for sampling biases in the retrievals due to incomplete coverage of the measurements. This was done following the sampling of the BIRA/KNMI and Dalhousie/SAO retrievals. Over regions dominated by biomass burning such biases are almost entirely caused by correlations between NO_2 abundance and cloud cover on seasonal time scales. Lack of observations during the wet seasons due to the presence of clouds introduces a positive bias of up to 30–50% in the retrieved annual means.

More serious are sampling biases from correlations at synoptic time scales shorter than a month, which also affect the retrieved monthly means. As these can only be accounted for in CTMs driven by assimilated meteorology, we distinguished two classes of models in our comparison. The first (ensemble A) consists of the CTMs that used

meteorology for the year of interest (2000) and provided daily 10:30 local time (or hourly) output fields; the second (ensemble B) includes the CCMs and the other CTMs. Based on the A-ensemble model simulations, we estimated that correlations on daily to monthly time scales give rise to biases between –25% and +10% in the monthly NO_2 columns over the industrial regions of the eastern United States, Europe, and eastern China, explaining a large part of the total sampling bias over these regions (negative down to between –50% and –20%).

We presented maps of the annual mean tropospheric NO_2 column density for individual models and retrievals. By smoothing the data to a common resolution of $5^\circ \times 5^\circ$, the correlation between the modeled and retrieved spatial patterns improved systematically. The resulting correlation coefficients are high. With the exception of the model with the coarsest resolution, the spatial correlation coefficients for the region between 50° S and 65° N are in the range 0.86–0.93 for the BIRA/KNMI retrieval, 0.85–0.93 for the Bremen retrieval, and 0.82–0.88 for the Dalhousie/SAO retrieval.

We also compared the ensemble means of the models and retrievals and calculated the associated standard deviations. On average the models underestimate the retrievals in industrial regions and overestimate the retrievals in regions dominated by biomass burning. The strongest underestimations are found over the Bejing area of eastern China (up to 6.0×10^{15} molecules cm^{-2}) as well as over the Highveld region of South Africa and over Western Europe south of Scandinavia (up to 4.0×10^{15} molecules cm^{-2}). Smaller underestimations are found over the eastern United States, California, the Persian Gulf, India, Hong Kong, South Korea and Japan. The strongest overestimations (up to 1.5×10^{15} molecules cm^{-2}) are found over the savanna regions of Brazil south of the Amazon basis and over Angola. The models further overestimate the retrievals over Zambia and the southern Congo, over the south coast of West Africa, over the Central African Republic and southern Sudan, as well as over Southeast Asia. Simulated columns are also higher than retrieved over the North Atlantic, Ireland, Scotland, Scandinavia and the Baltic States.

However, there are significant differences among the three retrievals and among the

various models. Over industrial regions the spread in absolute column abundances is comparable to or larger among the retrievals than among the models. The differences among the retrievals are especially large over Southeast Asia and South Africa, where the relative standard deviation in the annual mean is 42.7% and 35.4%, respectively. Theoretical error propagation studies performed by the retrieval groups (Boersma et al., 2004; Martin et al., 2002, 2003b) indicate that the uncertainty of individual observations is on the order of 35–60% over regions with a large contribution of the troposphere to the total column. With standard deviations of 10–50% in the annual mean over polluted regions, the observed differences among the retrievals therefore imply that the retrieval errors have a large systematic component, such as resulting from assumptions on clouds, surface albedo, profile shape and aerosols.

Standard deviations are significantly larger for the full model ensemble than for the subset of models from ensemble A. The ensemble average NO_2 distributions on the other hand are very similar. The most pronounced differences are observed over the oceans and over remote regions, where the full ensemble produces a more diffuse pattern than the restricted ensemble A.

The seasonal cycle in tropospheric NO_2 was analyzed for eight regions of the world. Over the industrial regions the spread among the retrievals was found to be particularly pronounced in wintertime. The wintertime bias between the models and the retrievals over industrial regions is smallest for the Dalhousie/SAO retrieval. Also the ensemble average discrepancy between models and retrievals is dominated by the fact that the models do not reproduce the high wintertime values seen in the retrievals from BIRA/KNMI and Bremen. Especially over eastern China none of the models reproduce the strong wintertime enhancement seen in the European retrievals. These results suggest that the IIASA/EDGAR3.2 emissions from eastern China are significantly too low, especially in wintertime.

Over the Highveld region of South Africa a strong discrepancy is found throughout the year, suggesting that the emissions from this region are systematically underestimated. Summertime as well as wintertime values seem to be underestimated over

the eastern United States. The assumption that the emissions from fuel combustion in the United States are aseasonal seems inconsistent with the European retrievals. However, the high wintertime values over industrial regions in these retrievals could potentially be due to a retrieval problem, as the conditions are not particularly favorable for satellite observations during winter (low sun, stable boundary layer, large aerosol concentrations). The relatively large spread among the retrievals prevents us from drawing more definite conclusions on the seasonality of the American and European emissions.

Over regions dominated by biomass burning, the timing of the seasonal cycle is generally well reproduced by the models. Tropospheric NO_2 amounts over Northern Africa south of the Sahara, South America and Southeast Asia reach their maxima simultaneously in models and retrievals. Only over Central Africa south of the Equator the models peak one to two months earlier than the retrievals. Despite systematic differences among the retrievals, it can be concluded the seasonal cycles over the African regions are significantly stronger in the models than in the retrievals, partly because the models underestimate the retrievals during the wet season. This suggests that the NO_x emissions from soils in these regions are higher than assumed in the models, supporting the conclusion of Jaeglé et al. (2004, 2005) on this point.

When we use the GFED emissions for the year 2000 instead of the 1997–2002 average values, we find only moderate changes over Africa, where interannual variability of biomass burning is relatively unimportant. Over South America on the other hand the year-2000 emissions give significantly reduced levels of pollution during the active dry season, more consistent with the retrievals.

The amplitude of the seasonal cycle over the biomass burning regions of Northern and Central Africa is improved when the models use emissions based on recently proposed emission factors, resulting in a 40% reduction of NO_x emissions from savanna fires. The concurrent reduction in the chemical production of ozone in addition leads to a closer agreement between modeled and measured surface ozone mixing ratios (Ellingsen et al., 2006[2]). The spatial pattern of tropospheric NO_2 over South America

is also better reproduced. Given the discrepancies among the retrievals, it is difficult to draw more definite conclusions on the validity of the updated emission factors compared to the old ones. This is particularly so over Southeast Asia, where significantly more pollution is seen in the BIRA/KNMI retrieval than in the other two retrievals and the results from the different sensitivity simulations all fall within the range of the retrievals.

The observed discrepancies between models and retrievals are not resolved by including vertical profile information from the models. The application of averaging kernels to 3-D model output removes only a fraction of the underestimation by the models of the retrieved columns over industrial regions and may even lead to enhanced discrepancies over some of the biomass burning regions.

Neither can the differences be explained by diurnal variations in anthropogenic emissions. From a sensitivity simulation with the TM4 model in which a diurnal cycle in the European emissions was assumed, we estimated that such variations lead to a reduction of the amount of tropospheric NO_2 over Europe at 10:30 local time by 2.5–4.1% depending on the month, despite large variations in the emissions. Thus the assumption of constant emissions in the models has introduced a positive bias in the simulated columns over industrial regions of at most a few percent.

The differences among the models and the relatively large discrepancies among the current state-of-the-art NO_2 retrievals have important implications for top-down estimation of NO_x emissions from satellite observations and indicate that the best estimates from inverse modeling studies as recently published by Martin et al. (2003b), Jaeglé et al. (2004, 2005) and Müller and Stavrakou (2005) are highly sensitive to the choice of model and retrieval.

The discrepancies among the retrievals are inherent to differences in the retrieval methods. Our conclusions are therefore relevant to tropospheric NO_2 retrievals from other instruments such as SCIAMACHY and OMI as well. Further investigation of the details of the different retrieval approaches seems necessary.

Acknowledgements. The lead author acknowledges support from the European Union project RETRO under contract number EVK2-CT-2002-00170. Coordination of this study was financed

by the European network of excellence ACCENT. N. H. Savage and J. A. Pyle would like to acknowledge the NERC Centres for Atmospheric Science (NCAS) for funding and supercomputer support.

References

Andreae, M. O. and Merlet, P.: Emission of trace gases and aerosols from biomass burning, Global Biogeochem. Cycles, 15(4), 955–966, doi:10.1029/2000GB001382, 2001.

Arellano Jr., A. F., Kasibhatla, P. S., Giglio, L., van der Werf, G. R., and Randerson, J. T.: Top-down estimates of global CO sources using MOPITT measurements, Geophys. Res. Lett., 31, L01104, doi:10.1029/2003GL018609, 2004.

Beirle, S., Platt, U., Wenig, M., and Wagner, T.: Weekly cycle of NO_2 by GOME measurements: a signature of anthropogenic sources, Atmos. Chem. Phys., 3, 2225–2232, 2003.

Beirle, S., Platt, U., Wenig, M., and Wagner, T.: Highly resolved global distribution of tropospheric NO_2 using GOME narrow swath mode data, Atmos. Chem. Phys., 4, 1913–1924, 2004.

Berntsen, T., Fuglestvedt, J. S., Joshi, M., Shine, K. P., Stuber, N., Sausen, R., Li, L., Hauglustaine, D. A., and Ponater, M.: Climate response to regional emissions of ozone precursors: sensitivities and warming potentials, Tellus B, 57, 283–304, 2005.

Bey, I., Jacob, D. J., Yantosca, R. M., et al.: Global modelling of tropospheric chemistry with assimilated meteorology: Model description and evaluation, J. Geophys. Res., 106, 23 073–23 095, 2001.

Boersma, K. F., Eskes, H. J., and Brinksma, E. J.: Error analysis for tropospheric NO_2 retrieval from space, J. Geophys. Res., 109, D04311, doi:10.1029/2003JD003962, 2004.

Brasseur, G. P., Hauglustaine, D. A., Walters, S., Rasch, P. J., Müller, J.-F., Granier, C., and Tie, X. X.: MOZART, a global chemical transport model for ozone and related chemical tracers: 1. Model description, J. Geophys. Res., 103, 28 265–28 289, 1998.

Burrows, J. P., Weber, M., Buchwitz, M., et al.: The Global Ozone Monitoring Experiment (GOME): Mission concept and first results, J. Atmos. Sci., 56, 151–175, 1999.

Chance, K.: Analysis of BrO measurements from the Global Ozone Monitoring Experiment, Geophys. Res. Lett., 25(17), 3335–3338, doi:10.1029/98GL52359, 1998.

Chipperfield, M. P.: Multiannual simulations with a three-dimensional chemical transport model, J. Geophys. Res., 104(D1), 1781–1806, doi:10.1029/98JD02597, 1999.

Cofala, J., Amann, M., and Mechler, R.: Scenarios of world anthropogenic emissions of air pollutants and methane up to 2030, Report of the Transboundary Air Pollution (TAP) programme, International Institute for Applied Systems Analysis, Laxenburg, Austria, 2005.

de Haan, J. F., Bosma, P. B., and Hovenier, J. W.: The adding method for multiple scattering calculations of polarized light, Astron. Astrophys., 183, 371–391, 1987.

Dentener, F. J. and Crutzen, P. J.: Reaction of N_2O_5 on tropospheric aerosols: Impact on the global distribution of NO_x, O_3, and OH, J. Geophys. Res., 98, 7149–7163, 1993.

Dentener, F., Peters, W., Krol, M., van Weele, M., Bergamaschi, P., and Lelieveld, J.: Interannual variability and trend of CH_4 lifetime as a measure for OH changes in the 1979–1993 time period, J. Geophys. Res., 108(D15), 4442, doi:10.1029/2002JD002916, 2003.

Dentener, F., Stevenson, D., Cofala, J., Mechler, R., Amann, M., Bergamaschi, P., Raes, F., and Derwent, R.: The impact of air pollutant and methane emission controls on tropospheric ozone and radiative forcing: CTM calculations for the period 1990–2030, Atmos. Chem. Phys., 5, 1731–1755, 2005.

Dentener, F., Stevenson, D., Ellingsen, K., van Noije, T., Schultz, M., et al.: The global atmospheric environment for the next generation, Environ. Sci. Technol., in press, 2006a.

Dentener, F., Drevet, J., Stevenson, D., Ellingsen, K., van Noije, T., Schultz, M., et al.: Nitrogen and sulfur deposition on regional and global scales: a multi-model evaluation, Global Biogeochem. Cycles, accepted, 2006b.

Dentener, F., Kinne, S., Bond, T., et al.: Emissions of primary aerosol and precursor gases in the years 2000 and 1750, prescribed data-sets for AeroCom, Atmos. Chem. Phys. Discuss., 6, 2703–2763, 2006c.

Derwent, R. G., Collins, W. J., Johnson, C. E., and Stevenson, D. S.: Transient behaviour of tropospheric ozone precursors in a global 3-D CTM and their indirect greenhouse effects, Climatic Change, 49, 463–487, 2001.

Duncan, B. N., Martin, R. V., Staudt, A. C., Yevich, R., and Logan, J. A.: Interannual and seasonal variability of biomass burning emissions constrained by satellite observations, J. Geophys. Res., 108(D2), 4100, doi:10.1029/2002JD002378, 2003.

Eskes, H. J. and Boersma, K. F.: Averaging kernels for DOAS total-column satellite retrievals, Atmos. Chem. Phys., 3, 1285–1291, 2003.

Evans, M. J. and Jacob, D. J.: Impact of new laboratory studies of N_2O_5 hydrolysis on global

model budgets of tropospheric nitrogen oxides, ozone, and OH, Geophys. Res. Lett., 32, L09813, doi:10.1029/2005GL022469, 2005.

Folberth, G. A., Hauglustaine, D. A., Lathière, J., and Brocheton, F.: Impact of biogenic hydrocarbons on tropospheric chemistry: results from a global chemistry-transport model, Atmos. Chem. Phys. Discuss., 5, 10 517–10 612, 2005.

Hallquist, M., Stewart, D. J., Baker, J., and Cox, R. A.: Hydrolysis of N_2O_5 on submicron sulfuric acid aerosols, J. Phys. Chem. A, 104, 3984–3990, 2000.

Hauglustaine, D. A., Brasseur, G. P., Walters, S., Rasch, P. J., Müller, J.-F., Emmons, L. K., and Carroll, M. A.: MOZART, a global chemical transport model for ozone and related chemical tracers: 2. Model results and evaluation, J. Geophys. Res., 103, 28 291–28 335, 1998.

Hauglustaine, D. A., Hourdin, F., Walters, S., Jourdain, L., Filiberti, M.-A., Larmarque, J.-F., and Holland, E. A.: Interactive chemistry in the Laboratoire de Météorologie Dynamique general circulation model: Description and background tropospheric chemistry evaluation, J. Geophys. Res., 109, D04314, doi:10.1029/2003JD003957, 2004.

Heland, J., Schlager, H., Richter, A., and Burrows, J. P.: First comparison of tropospheric NO_2 column densities retrieved from GOME measurements and in situ aircraft profile measurements, Geophys. Res. Lett., 29(20), 1983, doi:10.1029/2002GL015528, 2002.

Henderson, S. C., Wickrama, U. K., Baughcum, S. L., et al.: Aircraft emissions: current inventories and future scenarios, in: IPCC Special Report on Aviation and the Global Atmosphere, edited by: Penner, J. E., Lister, D. H., Griggs, D. J., and Dokken, D. J., McFarland, M., p. 290–331, Cambridge University Press, United Kingdom, 1999.

Herman, J. R. and Celarier, E. A.: Earth surface reflectivity climatology at 340–380 nm from TOMS data, J. Geophys. Res., 102(D23), 28 003–28 012, 1997.

Horowitz, L. W., Walters, S., Mauzerall, D. L., Emmons, L. K., Rasch, P. J., Granier, C., Tie, X., Lamarque, J.-F., Schultz, M. G., Tyndall, G. S., Orlando, J. J., and Brasseur, G. P.: A global simulation of tropospheric ozone and related tracers: Description and evaluation of MOZART, version 2, J. Geophys. Res., 108, 4784, doi:10.1029/2002JD002853, 2003.

Irie, H., Sudo, K., Akimoto, H., et al.: Evaluation of long-term tropospheric NO_2 data obtained by GOME over East Asia in 1996–2002, Geophys. Res. Lett., 32, L11810, doi:10.1029/2005GL022770, 2005.

Isaksen, I., Jackman, C. H., et al.: Modeling the chemical composition of the future atmosphere, in: IPCC Special Report on Aviation and the Global Atmosphere, edited by: Penner, J. E., Lister, D. H., Griggs, D. J., Dokken, D. J., and McFarland, M., p. 121–164, Cambridge

University Press, United Kingdom, 1999.

Ito, A. and Penner, J. E.: Global estimates of biomass burning emissions based on satellite imagery for the year 2000, J. Geophys. Res., 109, D14S05, doi:10.1029/2003JD004423, 2004.

Jaeglé, L., Martin, R. V., Chance, K., Steinberger, L., Kurosu, T. P., Jacob, D. J., Modi, A. I., Yoboué, V., Sigha-Nkamdjou, L., and Galy-Lacaux, C.: Satellite mapping of rain-induced nitric oxide emissions from soils, J. Geophys. Res., 109, D21310, doi:10.1029/2004JD004787, 2004.

Jaeglé, L., Steinberger, L., Martin, R. V., and Chance, K.: Global partitioning of NO_x sources using satellite observations: Relative roles of fossil fuel combustion, biomass burning and soil emissions, Faraday Discuss., 130, 407–423, 2005.

Konovalov, I. B., Beekmann, M., Vautard, R., Burrows, J. P., Richter, A., Nüß, H., Elansky, N.: Comparison and evaluation of modelled and GOME measurement derived tropospheric NO_2 columns over Western and Eastern Europe, Atmos. Chem. Phys., 5, 169–190, 2005.

Koelemeijer, R. B. A., Stammes, P., Hovenier, J. W., and de Haan, J. F.: A fast method for retrieval of cloud parameters using oxygen a band measurements from the Global Ozone Monitoring Experiment, J. Geophys. Res., 106(D4), 3475–3490, doi:10.1029/2000JD900657, 2001.

Koelemeijer, R. B. A., de Haan, J. F., and Stammes, P.: A database of spectral surface reflectivity in the range 335–772 nm derived from 5.5 years of GOME observations, J. Geophys. Res., 108(D2), 4070, doi:10.1029/2002JD002429, 2003.

Krol, M., Houweling, S., Bregman, B., van den Broek, M., Segers, A., van Velthoven, P., Peters, W., Dentener, F., and Bergamaschi, B.: The two-way nested global chemistry-transport zoom model TM5: algorithm and applications, Atmos. Chem. Phys., 5, 417–432, 2005.

Kunhikrishnan, T., Lawrence, M. G., von Kuhlmann, R., Richter, A., Ladstätter-Weißenmayer, A., and Burrows, J. P.: Analysis of tropospheric NO_x over Asia using the model of atmospheric transport and chemistry (MATCH-MPIC) and GOME-satellite observations, Atmos. Environ., 38, 581–596, 2004a.

Kunhikrishnan, T., Lawrence, M. G., von Kuhlmann, R., Richter, A., Ladstätter-Weißenmayer, A., and Burrows, J. P.: Semiannual NO_2 plumes during the monsoon transition periods over the central Indian Ocean, Geophys. Res. Lett., 31, L08110, doi:10.1029/2003GL019269, 2004b.

Kurosu, T. P., Chance, K., and Spurr, R. J. D.: CRAG – Cloud retrieval algorithm for the Eu-

ropean Space Agency's Global Ozone Monitoring Experiment, ESA WPP-161, p. 513–521, European Space and Technology Centre, Noordwijk, The Netherlands, 1999.

Lamarque, J.-F., Kiehl, J. T., Hess, P. G., Collins, W. D., Emmons, L. K., Ginoux, P., Luo, C., and Tie, X. X.: Response of a coupled chemistry-climate model to changes in aerosol emissions: Global impact on the hydrological cycle and the tropospheric burdens of OH, ozone and NO_x, Geophys. Res. Lett., 32, L16809, doi:10.1029/2005GL023419, 2005.

Law, K. S., Plantevin, P.-H., Shallcross, D. E., Rogers H. L., Pyle, J. A., Grouhel, C., Thouret, V., and Marenco, A.: Evaluation of modeled O_3 using Measurement of Ozone by Airbus In-Service Aircraft (MOZAIC) data, J. Geophys. Res., 103, 25 721–25 737, 1998.

Law, K. S., Plantevin, P.-H., Thouret, V., Marenco, A., Asman, W. A. H., Lawrence, M., Crutzen P. J., Müller, J.-F., Hauglustaine, D. A., and Kanakidou, M.: Comparison between global chemistry transport model results and Measurement of Ozone by Airbus In-Service Aircraft (MOZAIC) data, J. Geophys. Res., 105, 1503–1525, 2000.

Lawrence, M. G., Crutzen, P. J., Rasch, P. J., Eaton, B. E., and Mahowald, N. M.: A model for studies of tropospheric photochemistry: Description, global distributions, and evaluation. J. Geophys. Res., 104, 26 245–26 277, 1999.

Leue, C., Wenig, M., Wagner, T., Klimm, O., Platt, U., and Jähne, B.: Quantitative analysis of NO_x emissions from Global Ozone Monitoring Experiment satellite image sequences, J. Geophys. Res., 106(D6), 5493–5506, 2001.

Lauer, A., Dameris, M., Richter, A., and Burrows, J. P.: Tropospheric NO_2 columns: a comparison between model and retrieved data from GOME measurements, Atmos. Chem. Phys., 2, 67–78, 2002.

Martin, R. V., Chance, K., Jacob, D. J., et al.: An improved retrieval of tropospheric nitrogen dioxide from GOME, J. Geophys. Res., 107(D20), 4437, doi:10.1029/2001JD001027, 2002.

Martin, R. V., Jacob, D. J., Yantosca, R. M., Chin, M., and Ginoux, P.: Global and regional decreases in tropospheric oxidants from photochemical effects of aerosols, J. Geophys. Res., 108(D3), 4097, doi:10.1029/2002JD002622, 2003a.

Martin, R. V., Jacob, D. J., Chance, K., Kurosu, T. P., Palmer, P. I., and Evans, M. J.: Global inventory of nitrogen oxide emissions constrained by space-based observations of NO_2 columns, J. Geophys. Res., 108(D17), 4537, doi:10.1029/2003JD003453, 2003b.

Martin R. V., Parrish, D. D., Ryerson, T. B., Nicks Jr., D. K., Chance, K., Kurosu, T. P., Jacob, D. J., Sturges, E. D., Fried, A., and Wert, B. P.: Evaluation of GOME satellite measurements of tropospheric NO_2 and HCHO using regional data from aircraft campaigns in the southeastern

United States, J. Geophys. Res., 109, D24307, doi:10.1029/2004JD004869, 2004.

Müller, J.-F. and Brasseur, G. P.: IMAGES: A three-dimensional chemical transport model of the global troposphere, J. Geophys. Res., 100, 16 445–16 490, 1995.

Müller, J.-F. and Stavrakou, T.: Inversion of CO and NO_x emissions using the adjoint of the IMAGES model, Atmos. Chem. Phys., 5, 1157–1186, 2005.

Olivier, J. G. J. and Berdowski, J. J. M.: Global emissions sources and sinks, in: The Climate System, edited by: Berdowski, J. J. M., Guicherit, R., and Heij, B. J., p. 33–78, A. A. Balkema Publishers/Swets & Zeitlinger Publishers, Lisse, The Netherlands, 2001.

Ordóñez, C., Richter, A., Steinbacher, M., Zellweger, C., Nüß, H., Burrows, J. P., and Prévôt, A. S. H.: Comparison between 7 years of satellite-borne and ground-based tropospheric NO_2 measurements around Milan, Italy, J. Geophys. Res., 111, D05310, doi:10.1029/2005JD006305, 2006.

Park R. J., Jacob, D. J., Chin, M., and Martin, R. V.: Sources of carbonaceous aerosols over the United States and implications for natural visibility, J. Geophys. Res., 108(D12), 4355, doi:10.1029/2002JD003190, 2003.

Park, R. J., Jacob, D. J., Field, B. D., Yantosca, R. M., and Chin, M.: Natural and transboundary pollution influences on sulfate-nitrate-ammonium aerosols in the United States: Implications for policy, J. Geophys. Res., 109, D15204, doi:10.1029/2003JD004473, 2004.

Petritoli, A., Bonasoni, P., Giovanelli, G., Ravegnani, F., Kostadinov, I., Bortoli, D., Weiss, A., Schaub, D., Richter, A., and Fortezza, F.: First comparison between ground-based and satellite-borne measurements of tropospheric nitrogen dioxide in the Po basin, J. Geophys. Res., 109, D15307, doi:10.1029/2004JD004547, 2004.

Pétron, G., Granier, C., Khattotov, B., Yudin, V., Lamarque, J.-F., Emmons, L., Gille, J., and Edwards, D. P.: Monthly CO surface sources inventory based on the 2000-2001 MOPITT satellite data, Geophys. Res. Lett., 31, L21107, doi:10.1029/2004GL020560, 2004.

Pitari, G., Mancini, E., Rizi, V., and Shindell, D. T.: Impact of future climate and emissions changes on stratospheric aerosols and ozone, J. Atmos. Sci., 59, 414–440, 2002.

Rasch, P. J., Mahowald, N. M., and Eaton, B. E.: Representations of transport, convection and the hydrologic cycle in chemical transport models: Implications for the modeling of short lived and soluble species, J. Geophys. Res., 102, 28 127–28 138, 1997.

Richter, A. and Burrows, J. P.: Tropospheric NO_2 from GOME measurements, Adv. Space Res., 29, 1673–1683, 2002.

Richter, A., Burrows, J. P., Nüß, H., Clerbaux, C., Hadji-Lazaro, J., Turquety, S., and Granier, C.:

Satellite observations of ozone precursors and ozone, POET Report#1, EU project EVK2-1999-00011, 2003.
Richter, A., Nüß, H., Burrows, J. P., Granier, C., and Niemeier, U.: Long term measurements of NO_2 and other tropospheric species from space, Proceedings of the XX Quadrennial Ozone Symposium, 1–8 June 2004, Kos, Greece, 213–214, 2004.
Richter, A., Burrows, J. P., Nüß, H., Granier, C., and Niemeier, U.: Increase in tropospheric nitrogen dioxide levels over China observed from space, Nature, 437, 129–132, 2005.
Rotman, D. A., Tannahill, J. R., Kinnison, D. E., et al.: Global Modeling Initiative assessment model: Model description, integration, and testing of the transport shell, J. Geophys. Res., 106(D2), 1669–1691, 2001.
Rotman, D. A., Atherton, C. S., Bergmann, D. J., et al.: IMPACT, the LLNL 3D global atmospheric chemical transport model for the combined troposphere and stratosphere: Model description and analysis of ozone and other trace gases, J. Geophys. Res., 109, D04303, doi:10.1029/2002JD003155, 2004.
Rozanov, V. V., Diebel, D., Spurr, R. J. D., and Burrows, J. P.: GOMETRAN: A radiative transfer model for the satellite project GOME, the plane-parallel version, J. Geophys. Res., 102(D14), 16 683–16 696, doi:10.1029/96JD01535, 1997.
Sadourny, R. and Laval, K.: January and July performance of the LMD general circulation model, in: New Perspectives in Climate Modeling, edited by: Berger, A. and Nicolis, C., p. 173–197, Elsevier, 1984.
Savage, N. H., Law, K. S., Pyle, J. A., Richter, A., Nüß, H., and Burrows, J. P.: Using GOME NO2 satellite data to examine regional differences in TOMCAT model performance, Atmos. Chem. Phys., 4, 1895–1912, 2004.
Solomon, S., Portmann, R. W., Sanders, R. W., Daniel, J. S., Madsen, W., Bartram, B., and Dutton, E. G.: On the role of nitrogen dioxide in the absorption of solar radiation, J. Geophys. Res., 104(D10), 12 047–12 058, 1999.
Spurr, R. J. D., Kurosu, T. P., and Chance, K. V.: A linearized discrete ordinate radiative transfer model for atmospheric remote sensing retrieval, J. Quant. Spectrosc. Radiat. Trans., 68, 689–735, 2001.
Spurr, R. J. D.: Simultaneous derivation of intensities and weighting functions in a general pseudo-spherical discrete ordinate radiative transfer treatment, J. Quant. Spectrosc. Radiat. Trans., 75, 129–175, 2002.
Stammes, P., de Haan, J. F., and Hovenier, J. W.: The polarized internal radiation field of a

planetary atmosphere, Astron. Astrophys., 225, 239–259, 1989.
Stevenson, D. S., Dentener, F. J., Schultz, M. G., Ellingsen, K., van Noije, T. P. C., Wild, O., Zeng, G., et al.: Multi-model ensemble simulations of present-day and near-future tropospheric ozone, J. Geophys. Res., in press, 2006.
Streets, D. G., Bond, T. C., Carmichael, G. R., et al.: An inventory of gaseous and primary aerosol emissions in Asia in the year 2000, J. Geophys. Res., 108(D21), 8809, doi:10.1029/2002JD003093, 2003.
Sudo, K., Takahashi, M., Kurokawa, J., and Akimoto, H.: CHASER: A global chemical model of the troposphere 1. Model description, J. Geophys. Res., 107(D17), 4339, doi:10.1029/2001JD001113, 2002a.
Sudo, K., Takahashi, M., and Akimoto, H.: CHASER: A global chemical model of the troposphere 2. Model results and evaluation, J. Geophys. Res., 107(D21), 4586, doi:10.1029/2001/JD001114, 2002b.
Sudo, K., Takahashi, M., and Akimoto, H.: Future changes in stratosphere-troposphere exchange and their impacts on future tropospheric ozone simulations, Geophys. Res. Lett., 30(24), 2256, doi:10.1029/2003GL018526, 2003.
Sundet, J. K.: Model studies with a 3-D global CTM using ECMWF data, Ph.D. thesis., Dept. of Geophysics, University of Oslo, Norway, 1997.
Tie, X., Madronich, S., Walters, S., Edwards, D. P., Ginoux, P., Mahowald, N., Zhang, R., Lou, C., and Brasseur, G.: Assessment of the global impact of aerosols on tropospheric oxidants, J. Geophys. Res., 110, D03204, doi:10.1029/2004JD005359, 2005.
Vandaele, A. C., Fayt, C., Hendrick, F., et al.: An intercomparison campaign of ground-based UV-visible measurements of NO_2, BrO, and OClO slant columns: Methods of analysis and results for NO_2, J. Geophys. Res., 110, D08305, doi:10.1029/2004JD005423, 2005.
van der A, R. J., Peters, D. H. M. U., Eskes, H. J., Boersma, K. F., van Roozendael, M., de Smedt, I., and Kelder, H. M.: Detection of the trend and seasonal variation in tropospheric NO_2 over China, J. Geophys. Res., accepted, 2006.
van der Werf, G. R, Randerson, J. T., Collatz, G. J., and Giglio, L.: Carbon emissions from fires in tropical and subtropical ecosystems, Global Change Biology, 9, 547–562, 2003.
van der Werf, G. R., Randerson, J. T., Collatz, G. J., Giglio, L., Kasibhatla, P. S., Arellano, A. F. Jr., Olsen, S. C., and Kasischke, E. S.: Continental-scale partitioning of fire emissions during the 1997 to 2001 El Niño/La Niña period, Science, 303, 73–76, 2004.
van Noije, T. P. C., Eskes, H. J., van Weele, M., and van Velthoven, P. F. J.: Implications of

the enhanced Brewer-Dobson circulation in European Centre for Medium-Range Weather Forecasts reanalysis ERA-40 for the stratosphere-troposphere exchange of ozone in global chemistry-transport models, J. Geophys. Res., 109, D19308, doi:10.1029/2004JD004586, 2004.

van Noije, T. P. C., Segers, A. J., and van Velthoven, P. F. J.: Time series of the stratosphere-troposphere exchange of ozone simulated with reanalyzed and operational forecast data, J. Geophys. Res., 111, D03301, doi:10.1029/2005JD006081, 2006.

Velders, G. J. M., Granier, C., Portmann, R. W., Pfeilsticker, K., Wenig, M., Wagner, T., Platt, U., Richter, A., and Burrows, J. P.: Global tropospheric NO_2 column distributions: Comparing three-dimensional model calculations with GOME measurements, J. Geophys. Res., 106(D12), 12 643–12 660, 2001.

von Kuhlmann, R., Lawrence, M. G., Crutzen, P. J., and Rasch, P. J.: A model for studies of tropospheric ozone and non-methane hydrocarbons: Model description and ozone results, J. Geophys. Res., 108(D9), 4294, doi:10.1029/2002JD002893, 2003a.

von Kuhlmann, R., Lawrence, M. G., Crutzen, P. J., and Rasch, P. J.: A model for studies of tropospheric ozone and non-methane hydrocarbons: Model evaluation of ozone-related species, J. Geophys. Res., 108(D23), 4729, doi:10.1029/2002JD003348, 2003b.

Wang, Y. X., McElroy, M. B., Wang, T., and Palmer, P. I.: Asian emissions of CO and NO_x: Constraints from aircraft and Chinese station data, J. Geophys. Res., 109, D24304, doi:10.1029/2004JD005250, 2004.

Wild, O., Zhu, X., and Prather, M. J.: Fast-j: Accurate simulation of in- and below-cloud photolysis in tropospheric chemical models, J. Atmos. Chem., 37, 245–282, 2000.

Wild, O. and Prather, M. J.: Excitation of the primary tropospheric chemical mode in a global 3-D model, J. Geophys. Res., 105, 24 647–24 660, 2000.

Wild, O., Prather, M. J., and Akimoto, H.: Indirect long-term global radiative cooling from NO_x emissions, Geophys. Res. Lett., 28(9), 1719–1722, 2001.

Wild, O., Sundet, J. K., Prather, M. J., Isaksen, I. S. A., Akimoto, H., Browell, E. V., and Oltmans, S. J.: CTM ozone simulations for spring 2001 over the Western Pacific: Comparisons with TRACE-P lidar, ozonesondes and TOMS columns, J. Geophys. Res., 108(D21), 8826, doi:10.1029/2002JD003283, 2003.

Table 1. Anthropogenic NO_x emissions for the year 2000 assumed in this study.

Source category	Eastern U.S.	Europe	Eastern China	South Africa	Northern Africa	Central Africa	South America	Southeast Asia	Global total
Industrial	3.37	5.24	4.45	0.29	0.10	0.11	0.05	0.30	33.71
Domestic	0.43	0.80	0.33	0.01	0.32	0.13	0.01	0.03	4.88
Traffic	4.72	11.10	1.54	0.23	0.57	0.19	0.24	0.82	52.78

Values are given in Tg NO_2/yr.

Table 2. NO_x emissions from biomass burning from the Global Fire Emissions Database (GFED) averaged over the years 1997–2002 with emission factors (EF) from Andreae and Merlet (2001), and for the year 2000 with the same emission factors or the updated values from Andreae (personal communication, 2004).

Inventory	Eastern U.S.	Europe	Eastern China	South Africa	Northern Africa	Central Africa	South America	Southeast Asia	Global total
GFED 1997–2002	0.07	0.09	0.02	0.27	7.21	6.86	3.76	0.94	33.14
GFED 2000	0.08	0.15	0.02	0.26	7.84	7.13	1.92	0.53	29.71
GFED 2000, updated EF	0.06	0.09	0.01	0.15	5.05	4.85	1.54	0.34	20.00

Values are given in Tg NO_2/yr.

Table 3. Spatial correlation between the annual mean tropospheric NO_2 column density field of the individual models and retrievals, calculated at 0.5°×0.5° after smoothing the data to a common resolution of 5°×5°. The values in parentheses are the corresponding values calculated at 0.5°×0.5° before smoothing.

Region	Global		50° S–65° N		
Model/Retrieval	BIRA/KNMI	Bremen	BIRA/KNMI	Bremen	Dalhousie/SAO
GMI-CCM	0.88 (0.82)	0.81 (0.76)	0.89 (0.82)	0.85 (0.80)	0.86 (0.80)
GMI-DAO	0.89 (0.82)	0.83 (0.78)	0.89 (0.82)	0.86 (0.81)	0.87 (0.81)
GMI-GISS	0.88 (0.82)	0.84 (0.79)	0.88 (0.82)	0.87 (0.81)	0.86 (0.80)
IMAGES	0.87 (0.80)	0.86 (0.80)	0.87 (0.80)	0.88 (0.82)	0.84 (0.78)
IMPACT	0.87 (0.80)	0.84 (0.78)	0.87 (0.80)	0.86 (0.80)	0.82 (0.76)
MATCH-MPIC	0.88 (0.81)	0.85 (0.79)	0.88 (0.81)	0.87 (0.81)	0.82 (0.76)
NCAR	0.86 (0.80)	0.87 (0.81)	0.86 (0.79)	0.88 (0.83)	0.83 (0.77)
ULAQ	0.79 (0.71)	0.79 (0.72)	0.77 (0.70)	0.80 (0.73)	0.75 (0.68)
CHASER	0.91 (0.86)	0.90 (0.86)	0.90 (0.85)	0.92 (0.88)	0.85 (0.81)
CTM2	0.89 (0.83)	0.89 (0.85)	0.88 (0.83)	0.90 (0.86)	0.83 (0.78)
FRSGC/UCI	0.90 (0.85)	0.90 (0.86)	0.90 (0.85)	0.92 (0.88)	0.85 (0.80)
GEOS-CHEM	0.91 (0.85)	0.88 (0.83)	0.91 (0.84)	0.90 (0.85)	0.87 (0.81)
LMDz-INCA	0.90 (0.86)	0.91 (0.87)	0.90 (0.85)	0.93 (0.89)	0.87 (0.83)
MOZ2-GFDL	0.91 (0.87)	0.91 (0.87)	0.91 (0.87)	0.92 (0.89)	0.86 (0.82)
p-TOMCAT	0.92 (0.87)	0.92 (0.88)	0.91 (0.86)	0.93 (0.89)	0.88 (0.83)
TM4	0.93 (0.89)	0.90 (0.87)	0.93 (0.89)	0.92 (0.89)	0.87 (0.84)
TM5	0.92 (0.89)	0.90 (0.87)	0.92 (0.88)	0.92 (0.88)	0.86 (0.83)

Table 4. Ensemble means and corresponding standard deviations of the annual mean tropospheric NO_2 column densities for the different regions.

Ensemble	Eastern U.S.	Europe	Eastern China	South Africa	Northern Africa	Central Africa	South America	Southeast Asia
Ensemble A+B	4.52±1.19 (26.3%)	2.51±.675 (26.9%)	3.83±1.13 (29.6%)	1.84±.498 (27.1%)	1.20±.289 (24.1%)	1.42±.362 (25.4%)	1.28±.353 (27.5%)	1.79±.501 (28.1%)
Ensemble A	4.63±.844 (18.2%)	2.44±.428 (17.5%)	4.09±.728 (17.8%)	1.89±.494 (26.1%)	1.14±.144 (12.6%)	1.36±.298 (21.9%)	1.22±.284 (23.1%)	1.83±.517 (28.2%)
Retrievals	6.28±.851 (13.5%)	2.75±.424 (15.4%)	6.43±.922 (14.3%)	5.59±1.98 (35.4%)	1.12±.325 (29.0%)	1.24±.193 (15.6%)	.717±.203 (28.3%)	1.27±.542 (42.7%)

Values are given in 10^{15} molecules cm^{-2}.

Table 5. Corrected annual mean tropospheric NO_2 column densities for the different regions, derived by averaging the monthly mean values (weighted by the number of days per month). Values obtained by application of the averaging kernels are given in parentheses.

Model/Retrieval	Eastern U.S.	Europe	Eastern China	South Africa	Northern Africa	Central Africa	South America	Southeast Asia
GMI-CCM	3.81	1.88	2.81	1.46	.886	1.06	.829	1.41
GMI-DAO	3.40	1.77	3.09	1.41	.796	.996	.773	1.28
GMI-GISS	3.61	1.80	2.72	1.33	.824	.994	.941	1.26
IMAGES	3.94	2.76	3.65	1.47	.973	1.31	1.04	1.43
IMPACT	3.87	2.11	3.28	1.16	.959	1.03	1.17	1.42
MATCH-MPIC	4.67	2.64	3.91	1.78	1.26	1.50	1.47	1.96
NCAR	8.09	4.41	7.09	2.51	1.79	2.05	1.82	2.57
ULAQ	3.71	3.70	2.16	1.02	1.15	1.32	.919	1.27
CHASER	3.61	1.96	3.14	1.33	.790	.877	.813	1.11
CTM2	6.40	3.41	5.80	2.23	1.11	1.62	1.59	2.58
FRSGC/UCI	4.72	2.62	4.12	1.76	.909	1.15	.986	1.71
GEOS-CHEM	4.08	2.29	3.73	1.51	.899	1.05	.798	1.57
LMDz-INCA	3.50 (3.69)	2.05 (2.24)	3.49 (4.08)	.957 (.985)	.828 (.766)	.814 (.623)	.930 (.695)	1.06 (.938)
MOZ2-GFDL	5.09	3.09	4.68	2.03	1.09	1.40	1.16	1.76
p-TOMCAT	4.83 (4.98)	2.61 (2.79)	4.07 (4.77)	1.80 (1.61)	.934 (.782)	1.12 (.747)	1.00 (.725)	1.48 (1.15)
TM4	4.37 (4.11)	2.25 (2.21)	4.02 (3.96)	1.65 (1.57)	.983 (.945)	1.16 (.929)	.896 (.775)	1.46 (1.19)
TM5	4.90	2.50	4.19	1.15	1.01	1.15	.998	1.70
Ensemble A+B	4.51	2.58	3.88	1.56	1.01	1.21	1.07	1.59
Ensemble A	4.61	2.53	4.14	1.60	.950	1.15	1.02	1.60
BIRA/KNMI	6.87	3.03	7.87	6.96	1.33	1.31	.836	1.66
Bremen	6.91	3.49	6.51	3.88	.776	.999	.540	.705
Dalhousie/SAO	5.26	2.32	5.51	4.37	1.02	1.09	.555	.922
Retrievals	6.35	2.95	6.63	5.07	1.04	1.13	.644	1.10

Values are given in 10^{15} molecules cm^{-2}.

Table 6. Spatial correlation between the annual mean tropospheric NO_2 column density over an extended region of South America (30° S–0° N×70° W–40° W) from the retrievals and from the TM4 model simulations with different biomass burning emissions, based on the Global Fire Emissions Database (GFED) averaged over the years 1997–2000 as well as specific for the year 2000 with or without updated emission factors (EF). The correlation coefficients have been calculated at 0.5°×0.5° after smoothing the data to a common resolution of 5°×5°. Averaging kernels have been applied to the model data.

Simulation	BIRA/KNMI	Bremen	Dalhousie/SAO
GFED 1997–2002	0.789	0.822	0.784
GFED 2000	0.806	0.852	0.826
GFED 2000, updated EF	0.823	0.865	0.836

Table A1. Overview of the GOME tropospheric NO_2 retrievals used in this study.

Retrieval aspect	BIRA/KNMI	University of Bremen	Dalhousie/SAO
Spectral fit	DOAS (426.3–451.3 nm)	DOAS (425–450 nm)	Direct spectral fit (426–452 nm)
Stratosphere-troposphere separation	Data assimilation in the TM4 model	Reference sector method: stratospheric contribution from daily output at GOME overpass time from the SLIMCAT model, scaled to the GOME slant columns over the Pacific Ocean (180°–210°); no further correction applied – tropospheric excess method (TEM)	Reference sector method: zonally invariant stratospheric contribution from the GOME slant columns over the central Pacific; tropospheric residual corrected for the tropospheric NO_2 over the Pacific using daily output from the GEOS-CHEM model
Radiative transfer model	DAK	SCIATRAN	LIDORT
Profile shape	Collocated daily output at overpass time from the TM4 model (3°×2°)	Monthly means from a run of the MOZART-2 model for 1997 (2.8°×2.8°)	Collocated daily output at overpass time from the GEOS-CHEM model (2.5°×2.0°)
Cloud fraction	FRESCO	FRESCO	GOMECAT
Cloud pressure	FRESCO	Not used	GOMECAT
Cloud selection threshold	Cloud radiance fraction of 50%	Cloud fraction of 20%	Cloud radiance fraction of 50%
Correction for partly cloudy scenes	Included	Not included	Included
Surface albedo	TOMS/GOME	GOME	GOME
Aerosol correction	Not included	LOWTRAN aerosol types: maritime over ocean, rural over land and urban over regions with high CO_2 emissions in the EDGAR database	Collocated daily aerosol profiles at overpass time from the GEOS-CHEM model
Temperature dependence of the absorption cross section	Correction of the slant column density based on ECMWF temperature profiles	Not included	Dependence based on US Standard Atmosphere
Reference	Boersma et al. (2004)	Richter et al. (2005)	Martin et al. (2003b); the version used in this study is the release of May 2005, which uses an improved fitting algorithm

Table A2. Overview of the models.

Model	Institute	Contact author	Resolution (lon/lat/levels) Top level	Underlying meteorology	Soil/Lightning NO_x emissions (Tg N/yr)	Reaction probability for N_2O_5 hydrolysis	Atmospheric CH_4 lifetime (yr) (Stevenson et al., 2006)	References
CHASER	FRCGC/ JAMSTEC	Kengo Sudo	2.8°/2.8°/L32 3 hPa	CTM: ECMWF operational analysis data for 2000	5.5/5.0	0.1 on liquid aerosols, 0.01 on ice	8.42	Sudo et al. (2002a, b)
CTM2	University of Oslo	Kjerstin Ellingsen Michael Gauss	2.8°/2.8°/L40 10 hPa	CTM: ECMWF-IFS pieced-forecast data for 2000	5.6/5.0	0.1	10.33	Sundet (1997)
FRSGC/UCI	FRCGC/ JAMSTEC	Oliver Wild	2.8°/2.8°/L37 10 hPa	CTM: ECMWF-IFS pieced-forecast data for 2000	5.5/6.5	Not applicable: hydrolysis treated as a pseudo-gas-phase reaction	7.61	Wild and Prather (2000) Wild et al. (2003)
GEOS-CHEM	EPFL	Isabelle Bey Jérôme Drevet	5°/4°/L30 0.01 hPa	CTM: GEOS assimilated fields from NASA GMAO for 2000	6.7/3.7	Dependent on aerosol type, relative humidity and temperature (Evans and Jacob, 2005): 0.02 in global mean	10.17	Bey et al. (2001) Martin et al. (2003a) Park et al. (2004)
GMI-CCM	NASA Global Modeling Initiative	José Rodriguez Susan Strahan	5°/4°/L52 0.006 hPa	GCM: NCAR MACCM3	6.6/5.0	0.1	7.50	Rotman et al. (2001) Wild et al. (2000) Bey et al. (2001)
GMI-DAO	NASA Global Modeling Initiative	José Rodriguez Susan Strahan	5°/4°/L46 0.048 hPa	CTM: GEOS-2-DAS assimilated fields for March 1997–Feb 1998	6.7/5.0	0.1	7.64	Rotman et al. (2001) Wild et al. (2000) Bey et al. (2001)
GMI-GISS	NASA Global Modeling Initiative	José Rodriguez Susan Strahan	5°/4°/L23 0.017 hPa	GCM: GISS-2'	6.8/5.0	0.1	8.54	Rotman et al. (2001) Wild et al. (2000) Bey et al. (2001)
IMAGES	BIRA-IASB	Jean-Francois Müller	5°/5°/L25 50 hPa	CTM: monthly means from ECMWF ERA-40 reanalysis	8.0/3.0	0.1	8.12	Müller and Brasseur (1995) Müller and Stavrakou (2005)

Table A2. Continued.

Model	Institute	Contact author	Resolution (lon/lat/levels) Top level	Underlying meteorology	Soil/Lightning NO_x emissions (Tg N/yr)	Reaction probability for N_2O_5 hydrolysis	Atmospheric CH_4 lifetime (yr) (Stevenson et al., 2006)	References
IMPACT	LLNL	Cynthia Atherton Daniel Bergmann	5°/4°/L26 2 hPa	GCM: CAM3	5.5/5.0	0.1	7.18	Rotman et al. (2004)
LMDz-INCA	LSCE	Didier Hauglustaine Sophie Szopa	3.75°/2.5°/L19 3 hPa	CTM: nudged to ECMWF ERA-40 reanalysis data for 2000	5.5/5.0	Temperature dependence from Hallquist et al. (2000): 0.185 at 200 K, 0.03 at 300 K	8.57	Sadourny and Laval (1984) Hauglustaine et al. (2004) Folberth et al. (2005)
MATCH	Max Planck Institute for Chemistry	Tim Butler Mark Lawrence	5.6°/5.6°/L28 2 hPa	CTM: NCEP/NCAR reanalysis data for 2000	7.0/5.0	0.05	9.48	von Kuhlmann et al. (2003a, b) Lawrence et al. (1999) Rasch et al. (1997)
MOZ2-GFDL	GFDL	Arlene Fiore Larry Horowitz	1.9°/1.9°/L28 0.7 hPa	CTM: NCEP/NCAR reanalysis data for 2000	6.1/6.0	0.04	8.42	Brasseur et al. (1998) Hauglustaine et al. (1998) Horowitz et al. (2003)
NCAR	NCAR	Jean-Francois Lamarque	2.8°/2.8°/L26 4 hPa	GCM: CCSM3	7.0/5.0	0.04	9.07	Horowitz et al. (2003) Tie et al. (2005) Lamarque et al. (2005) Emmons et al. (2006, in preparation)
p-TOMCAT	University of Cambridge	Nick Savage John Pyle	2.8°/2.8°/L31 10 hPa	CTM: ECMWF operational analysis data for 2000	5.5/3.9	Hydrolysis not included	12.46	Law et al. (1998, 2000)
TM4	KNMI	Twan van Noije	3°/2°/L25 0.48 hPa	CTM: ECMWF 3-6-h operational forecasts for 2000	6.0/7.0	0.04	8.80	Dentener et al. (2003) van Noije et al. (2004, 2006)
TM5	JRC	Frank Dentener Maarten Krol	6°/4°/L25 0.48 hPa (1°/1° Europe, N. America, and Asia)	CTM: ECMWF 3–6-h operational forecasts for 2000	5.8/5.0	0.04 on liquid aerosols, 0.01 on ice	7.93	Dentener et al. (2003) Krol et al. (2005)
ULAQ	Università L'Aquila	Veronica Montanaro Giovanni Pitari	22.5°/10°/L26 0.04 hPa	GCM: ULAQ-GCM	5.5/5.0	0.1	8.06	Pitari et al. (2002)

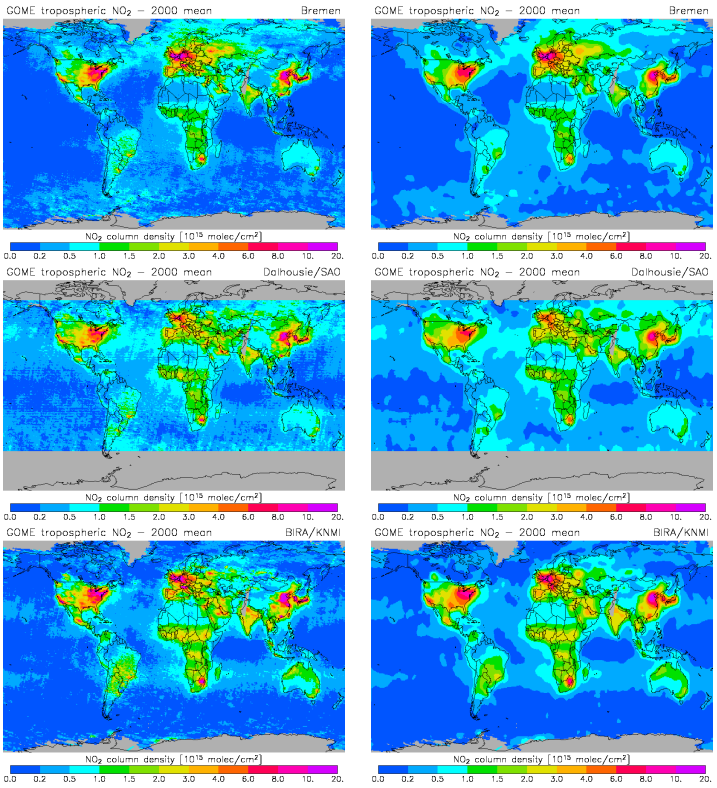

Fig. 1. Annual mean tropospheric NO_2 column density from the three retrievals. Data are shown on a horizontal resolution of 0.5°×0.5° (left) and smoothed to 5°×5° (right).

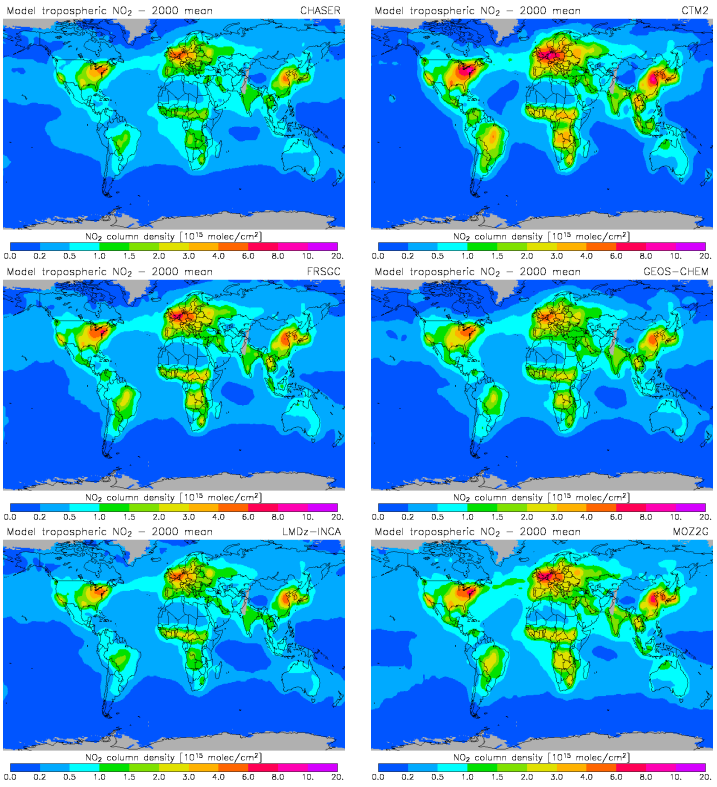

Fig. 2.

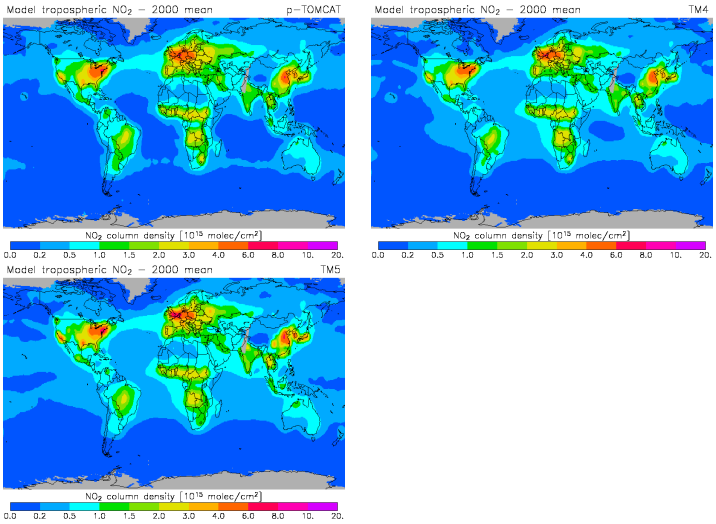

Fig. 2. Annual mean tropospheric NO_2 column density for the A-ensemble models. Data have been smoothed to a horizontal resolution of 5°×5°.

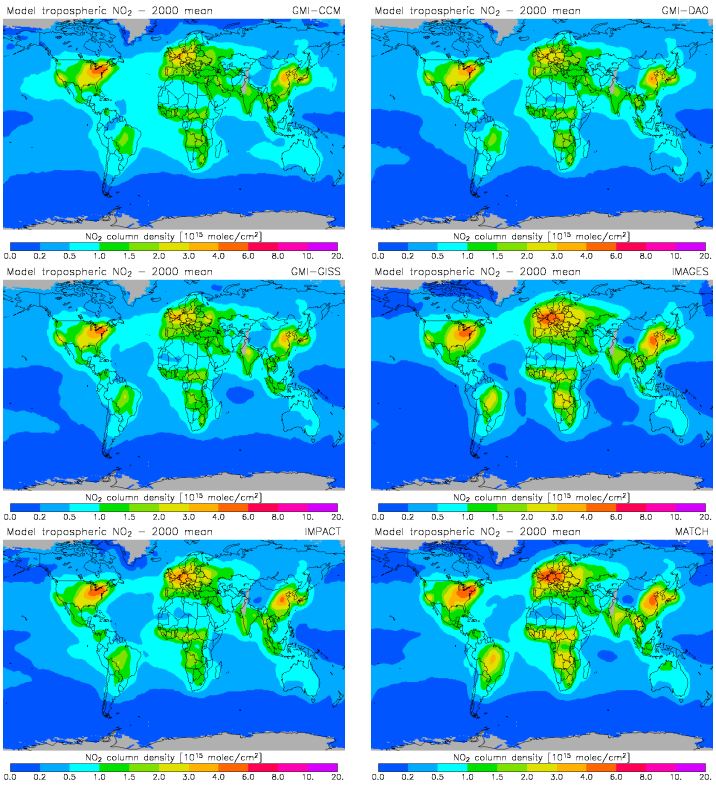

Fig. 3.

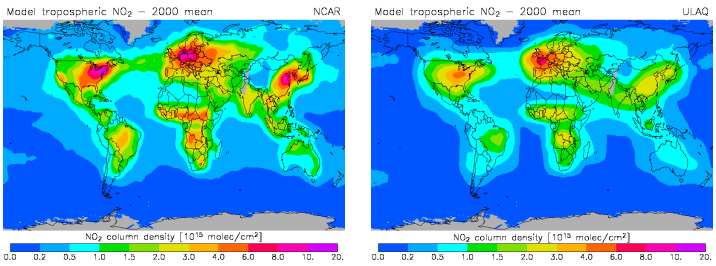

Fig. 3. Annual mean tropospheric NO_2 column density for the B-ensemble models. Data have been smoothed to a horizontal resolution of 5°×5°.

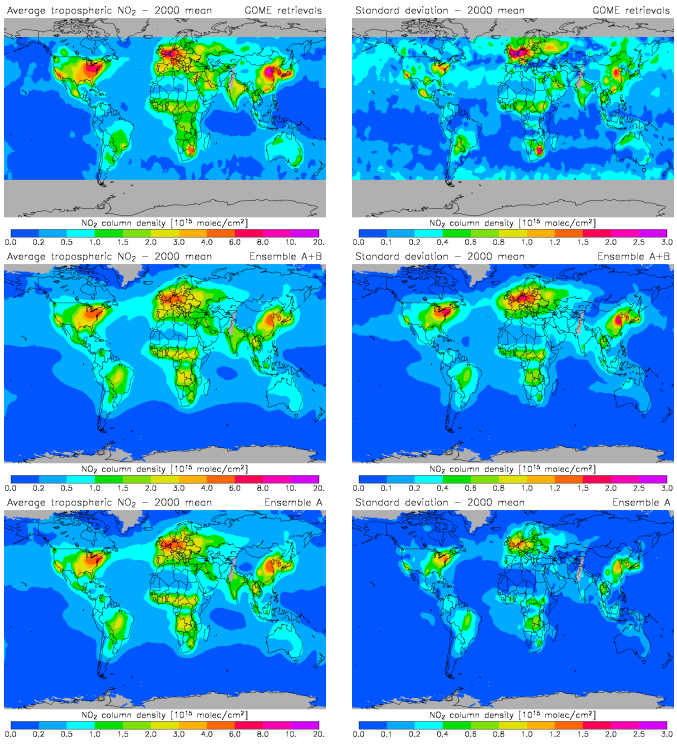

Fig. 4. Ensemble average annual mean tropospheric NO_2 column density with corresponding standard deviation for the three GOME retrievals, the full model ensemble (A+B), and ensemble A separately. These quantities have been calculated after smoothing the data to a horizontal resolution of 5°×5°.

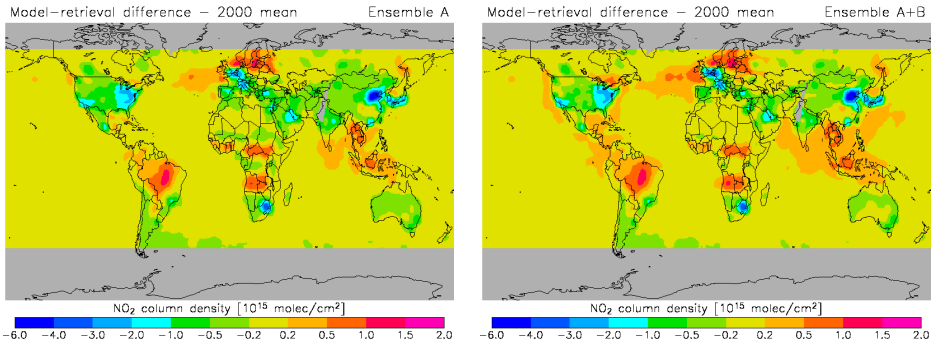

Fig. 5. Annual mean tropospheric NO_2 column density difference between models and retrievals for the full model ensemble (A+B) and ensemble A separately. Data have been smoothed to a horizontal resolution of 5°×5°.

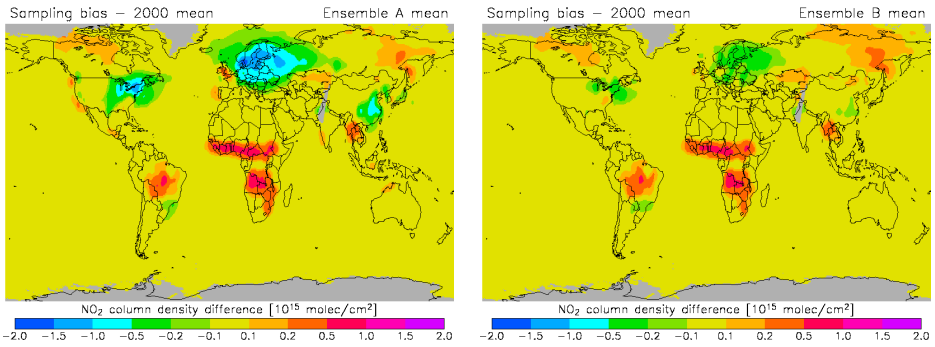

Fig. 6. Total sampling bias for ensembles A and B. Data have been smoothed to a horizontal resolution of 5°×5°.

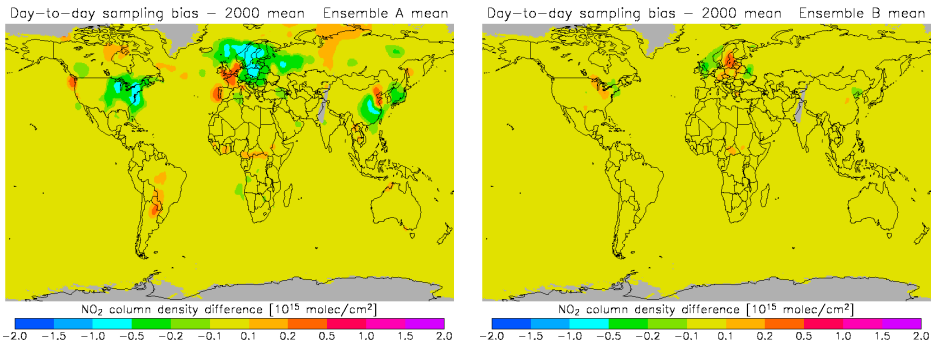

Fig. 7. Contribution of day-to-day variability to the sampling bias for ensembles A and B. Here the B-ensemble mean does not include the MATCH-MPIC and IMAGES models, which provided only monthly output. Data have been smoothed to a horizontal resolution of 5°×5°.

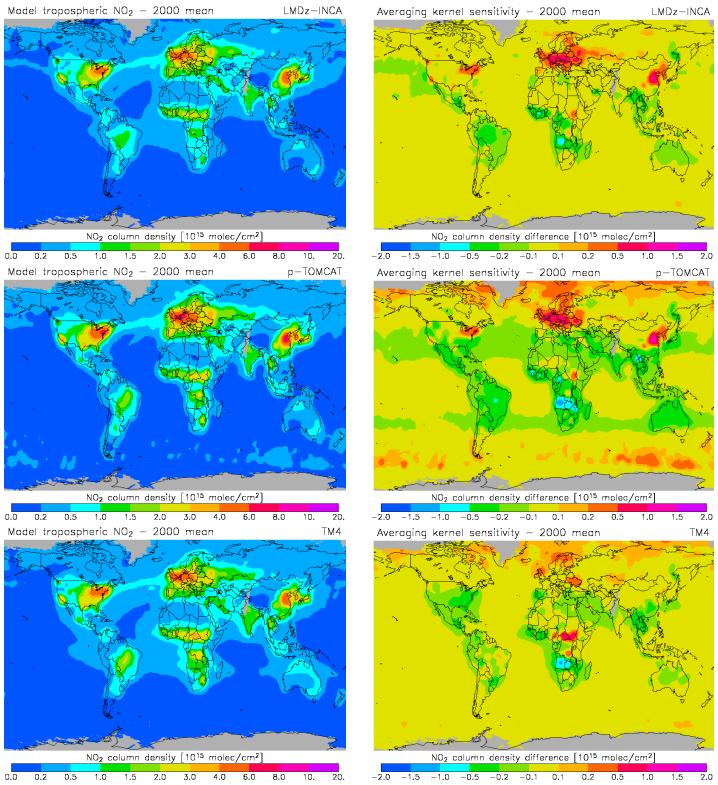

Fig. 8.

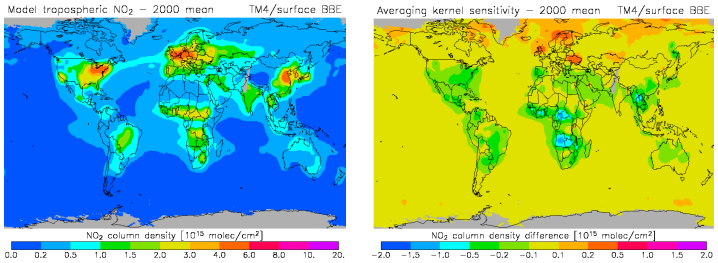

Fig. 8. Annual mean tropospheric NO_2 column density calculated by application of the averaging kernels to the daily 3-dimensional output fields from the three A-ensemble models LMDz-INCA, p-TOMCAT and TM4 (left), together with the difference compared to the corresponding fields shown in Fig. 2, obtained directly from the daily model columns (right). Results for the TM4 model in an alternative setup in which all biomass burning emissions (BBE) are released below 100 m, are included as well. Data have been smoothed to a horizontal resolution of 5°×5°.

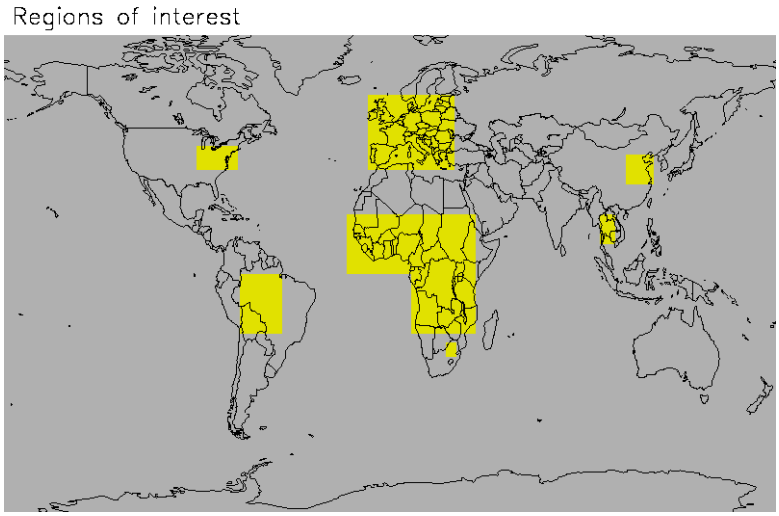

Fig. 9. Illustration of the various regions analyzed in this study: the eastern United States (90° W–71° W×35° N–43° N), Europe (10° W–30° E×35° N–60° N), eastern China (110° E–123° E×30° N–40° N), South Africa (26° E–31° E×28° S–23° S), Northern Africa (20° W–40° E×0° N–20° N), Central Africa (10° E–40° E×20° S–0° N), South America (70° W–50° W×20° S–0° N), and Southeast Asia (98° E–105° E×10° N–20° N).

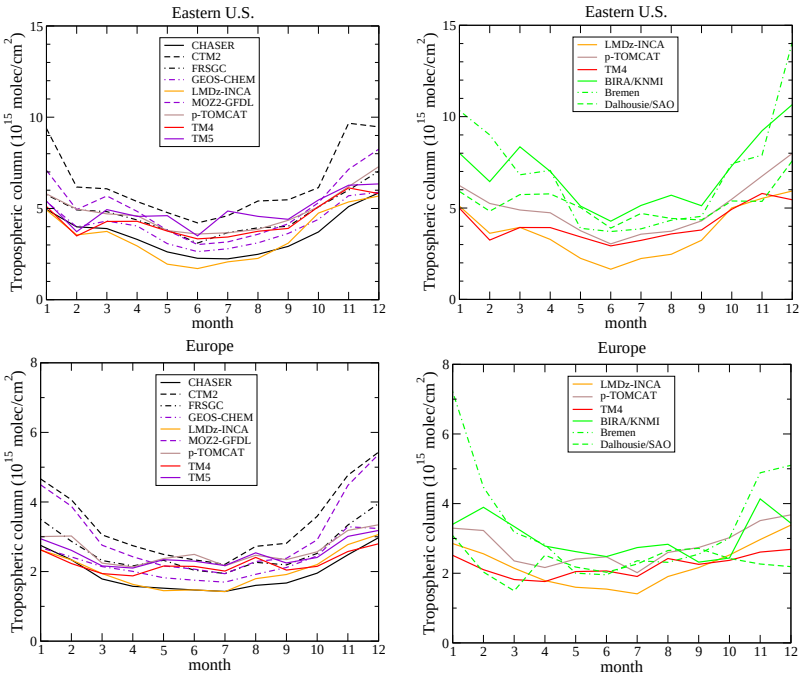
Eastern U.S.
Eastern U.S.
Europe
Europe
Tropospheric column (10^{15} molec/cm^2)
month
CHASER
CTM2
FRSGC
GEOS-CHEM
LMDz-INCA
MOZ2-GFDL
p-TOMCAT
TM4
TM5
LMDz-INCA
p-TOMCAT
TM4
BIRA/KNMI
Bremen
Dalhousie/SAO

Fig. 10.

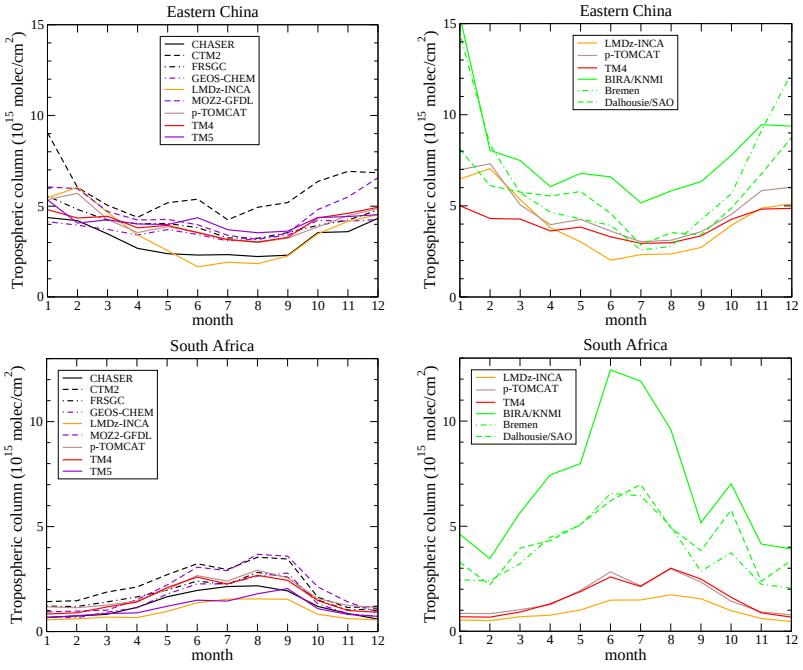
Eastern China
Eastern China
South Africa
South Africa
Tropospheric column (10^{15} molec/cm^2)
month
CHASER
CTM2
FRSGC
GEOS-CHEM
LMDz-INCA
MOZ2-GFDL
p-TOMCAT
TM4
TM5
LMDz-INCA
p-TOMCAT
TM4
BIRA/KNMI
Bremen
Dalhousie/SAO

Fig. 10.

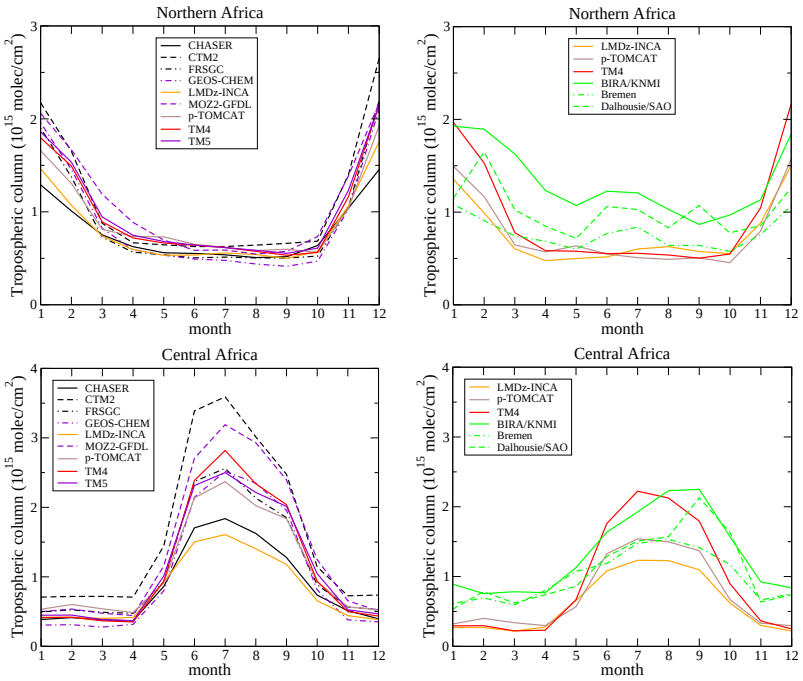

Fig. 10.

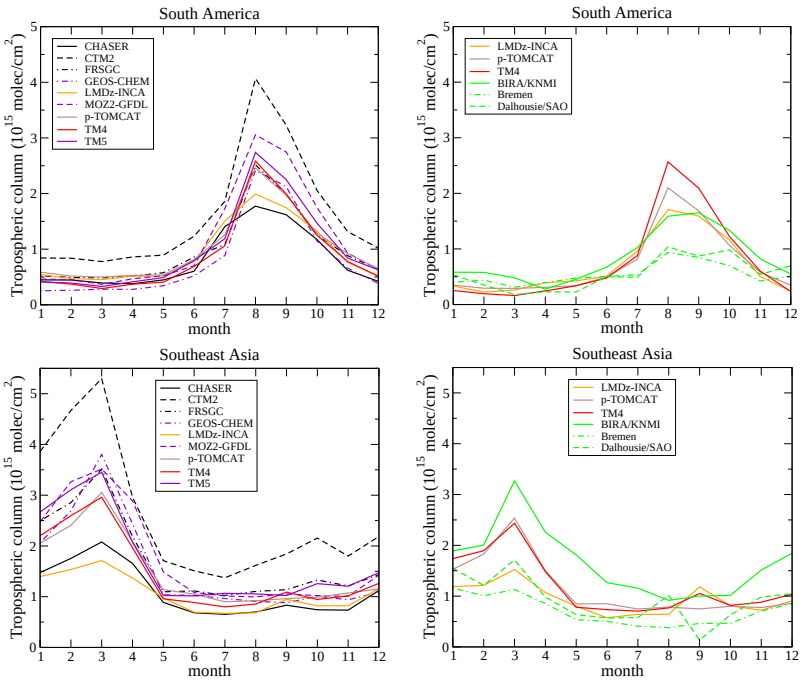

Fig. 10. Seasonal cycle in the tropospheric NO_2 column density for different regions of the world. Shown are the monthly values obtained from the daily column output from the A-ensemble models (left) or calculated by application of the averaging kernels to the daily 3-dimensional output fields from a subset of models (right), together with the corresponding retrieval data.

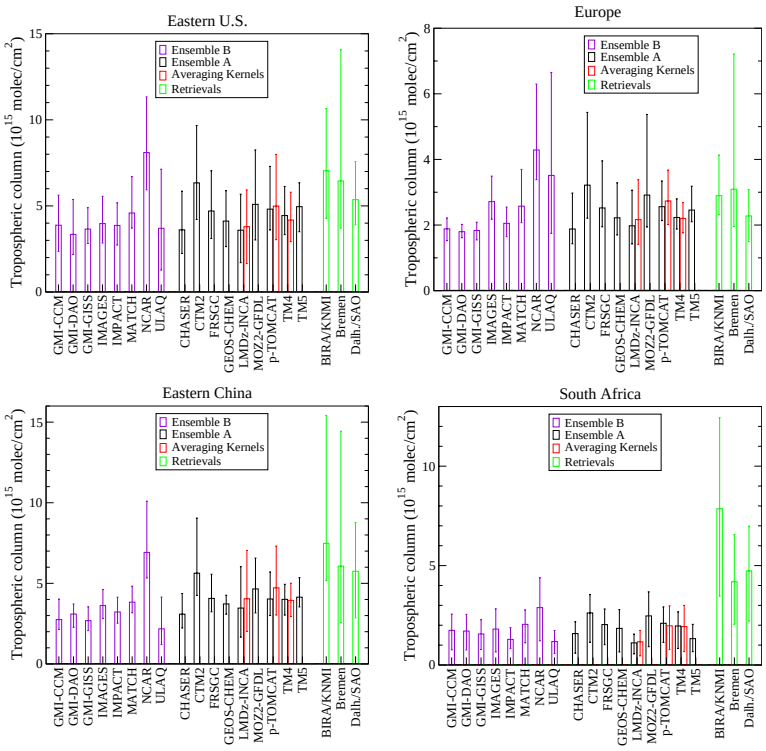

Fig. 11.

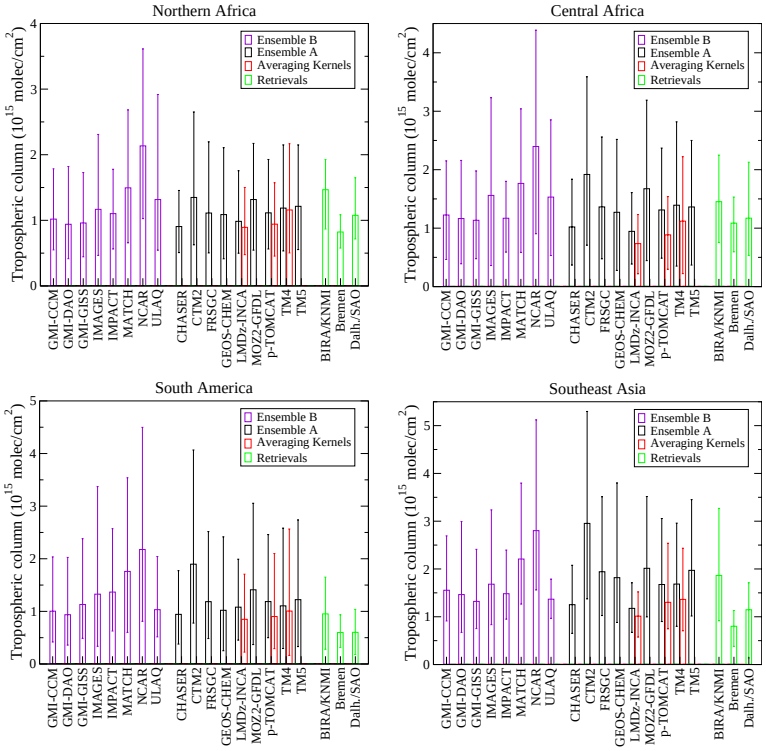

Fig. 11. Annual mean tropospheric NO_2 column density together with the minimum and maximum monthly mean values for the different world regions. Results calculated from the daily model columns ("Ensemble A", "Ensemble B") or the daily 3-dimensional output fields ("Averaging Kernels"), are compared to the corresponding retrieval data.

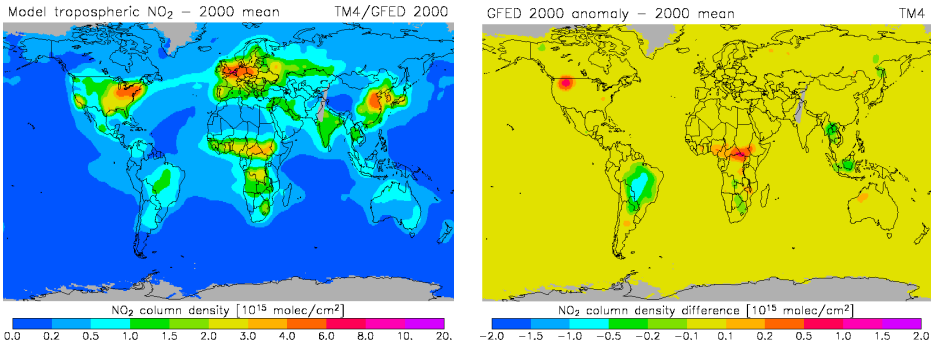

Fig. 12. Annual mean tropospheric NO_2 column density calculated with the TM4 model using GFED emissions for the year 2000 (left), together with the impact of using these emissions instead of the average GFED emissions for the years 1997–2002 (see corresponding map in Fig. 8). Averaging kernels have been applied; data have been smoothed to a horizontal resolution of 5°×5°.

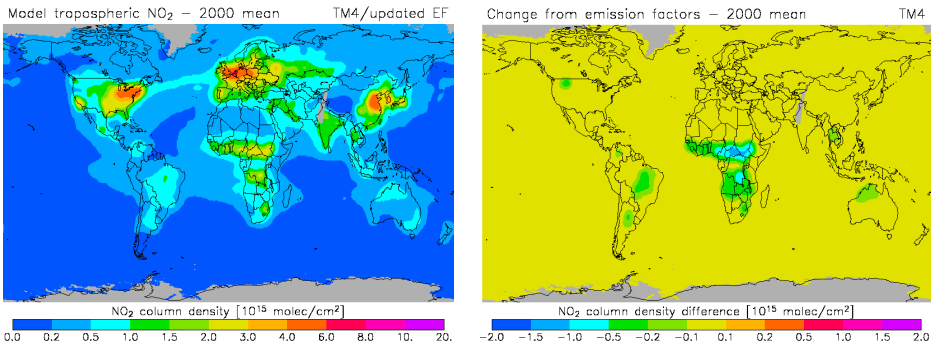

Fig. 13. Annual mean tropospheric NO_2 column density calculated with the TM4 model using GFED emissions for the year 2000 and updated emissions factors (EF) (left), together with the change resulting from using the updated values. Averaging kernels have been applied; data have been smoothed to a horizontal resolution of 5°×5°.

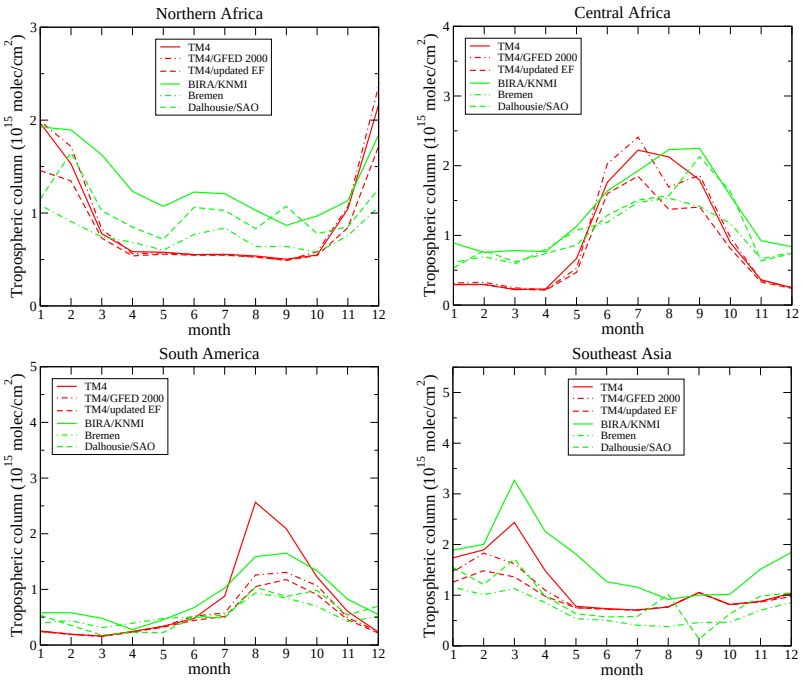

Fig. 14. Seasonal cycle in the tropospheric NO_2 column density for regions dominated by biomass burning. Shown are the monthly values calculated with the TM4 model using the average GFED emissions for the year 1997–2002 or the GFED emissions for the year 2000 with and without updated emission factors (EF), together with the corresponding retrieval data. Averaging kernels have been applied to the model data.

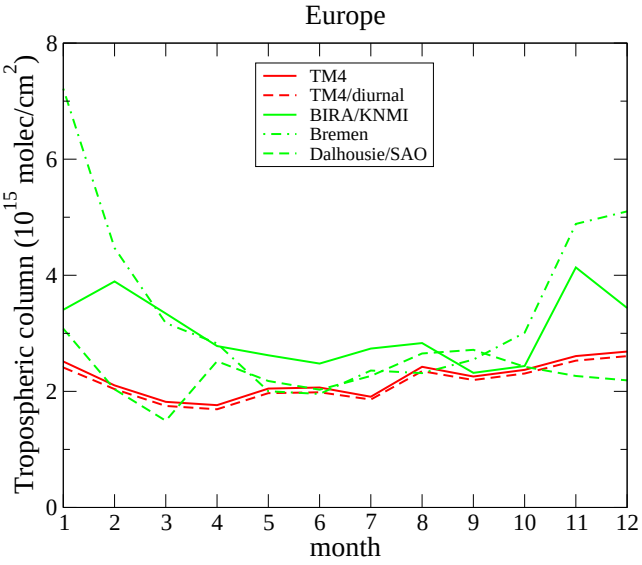

Fig. 15. Seasonal cycle in the tropospheric NO_2 column density for the European region. Shown are the monthly values calculated with the TM4 model with or without diurnal variations in the anthropogenic NO_x emissions in this region, together with the corresponding retrieval data. Averaging kernels have been applied to the model data.

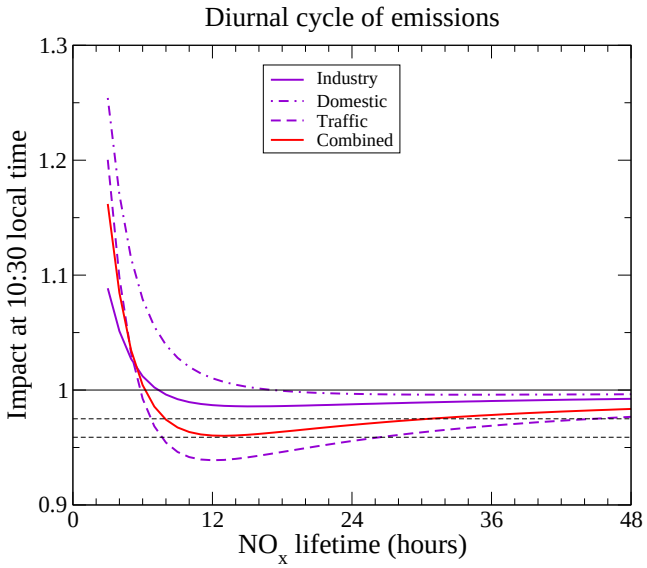

Fig. 16. Impact of diurnal variations in emissions on the tropospheric NO_2 column at 10:30 local time as a function of the lifetime of NO_x. Shown are the estimates for the separate anthropogenic emission source categories as well as for the combined anthropogenic emissions in the European region. The dashed black lines indicate the range obtained with the TM4 model.